DEVELOPMENTAL BIOLOGY

Notch controls APC/C^{FZR-1} to enable accumulation of chromatin regulators in germline stem cells from *Caenorhabditis elegans*

David Puerta[1,2], Sara Rivera-Martín[2], Adrián Fragoso-Luna[2], Susan Strome[3], Sarah L Crittenden[4], Judith Kimble[4], José Pérez-Martín[1,2]*

Originally known for its function in the cell cycle, the anaphase-promoting complex/cyclosome (APC/C) also plays a crucial role in regulating differentiation and maintaining cell identity. However, the mechanisms by which APC/C mediates developmental processes are not fully understood. In this study, we show that APC/C and its activator FZR-1 regulate the chromatin regulators MES-4 and MES-3. These proteins are part of histone methylation complexes essential for maintaining germline stem cell (GSC) identity in the germ line of *Caenorhabditis elegans*. APC/C^{FZR-1} facilitates the degradation of MES-4 and MES-3 when GSCs transition toward differentiating into oocytes. The activity of APC/C^{FZR-1} is restricted by the Notch signaling pathway provided by the distal tip cell, which is responsible for maintaining the stemness of the GSC pool. This negative regulation enables the accumulation of MES-3 and MES-4 in GSCs, offering an additional component by which niche activity modulates the *C. elegans* germ line.

INTRODUCTION

Stem cells maintain homeostasis in the body. Their ability to self-renew and differentiate into various cell types makes them promising sources for cell replacement therapies and regenerative medicine for treatment of injuries and diseases (*1*). Stem cells are typically found in specific tissue areas known as stem cell niches. These niches maintain the unique properties of stem cells. Understanding how niches maintain stem cell features may enable the manipulation of their regulatory mechanisms for future applications (*2*). However, the complex structure of mammalian tissues makes it challenging to identify and study the interactions between niches and stem cells in vivo. In contrast, invertebrate model systems have a simpler tissue architecture that facilitates the analysis of interactions between stem cells and their niches (*3*). These model systems provide convenient tools for genetic, cellular, and biochemical analyses of regulatory networks (*4*).

The germ line in *Caenorhabditis elegans* provides a simple model for studying stem cell regulation and the interaction of stem cells with their niche. It has similar features to mammalian stem cell niches and provides an effective platform for investigating key aspects of stem cell biology (*5*). The *C. elegans* germ line is enclosed in two U-shaped gonad arms. Germ cells in each arm are arranged distally to proximally in a specific spatiotemporal order [reviewed in (*6*)] (Fig. 1A). The distal tip cell (DTC), a somatic cell, occupies the distal tip of each gonad arm and acts as a stem cell niche to support nearby germ cells. The gonad area regulated by the niche is called the progenitor zone (PZ), which contains a pool of germline stem cells (GSCs) that divide mitotically and which extends for ~20 germline cell diameters (gcd) from the distal tip. The resulting divisions displace germ cells from the PZ into the transition zone (TZ), which extends for 8 to 10 gcd. The transition from the mitotic to the meiotic cell cycle begins just before the PZ/TZ boundary. After this boundary, germ cells progress through the first stages of meiotic prophase—leptotene, zygotene, and pachytene—and then differentiate into oocytes in the proximal arm. These oocytes remain arrested in diakinesis of meiotic prophase until fertilization, which occurs upon reaching the spermatheca in the most proximal region.

The DTC plays a central role in maintenance of the GSC pool. It signals through the Notch pathway and activates transcription of two key GSC regulators *lst-1* and *sygl-1*. LST-1 and SYGL-1 are both posttranscriptional regulators. LST-1 is also a transcriptional regulator that feeds back to Notch signaling (*7*). These regulators bind to each of the four PUF (Pumilio and FBF) proteins in the self-renewal PUF hub (*8*). Among the self-renewal PUF proteins, the nearly identical FBF-1 and FBF-2 play prominent roles. The resultant LST-1/PUF and SYGL-1/PUF complexes suppress the translation of mRNAs responsible for germline differentiation and somatic cell development (Fig. 1B).

GSCs in the PZ have a markedly short or nonexistent G_1 phase, owing to the sustained activity of the S-phase cyclin-dependent kinase 2 (CDK-2)/CYE-1 complex (*9*). CDK activity in the PZ is maintained by at least three mechanisms: (i) The glycogen synthase kinase ortholog glycogen synthase kinase 3 maintains elevated CDK-2 expression throughout the cell cycle (*10*); (ii) CYE-1 levels remain high due to the lack of protein degradation and continuous translation of its mRNA (*9*, *11*); and (iii) the germline CDK inhibitor CKI-2 is not translated in the PZ (*12*). The high CDK-2/CYE-1 activity typical of the PZ is down-regulated when cells enter the TZ, suggesting that niche activity supports CDK activity in the PZ. Two regulatory mechanisms responsible for maintaining high CDK activity in the PZ are controlled by the Notch pathway: inhibition of CKI-2 translation by FBF proteins (*12*) and translation of CYE-1 due to FBF-induced repression of GLD-1, a translational repressor of CYE-1 mRNA (*11*) (Fig. 1C).

In addition to cell cycle control, GSC maintenance requires the promotion of a germline-specific transcriptional program. MES-3 and MES-4 are abundant chromatin regulators in GSCs, but their levels markedly decrease when cells reach the TZ (*13*, *14*). MES-3

[1]Instituto de Biomedicina de Valencia (CSIC), Valencia, Spain. [2]Instituto de Biología Funcional y Genómica (CSIC), Salamanca, Spain. [3]Department of Molecular, Cell and Developmental Biology, University of California, Santa Cruz, Santa Cruz, CA, USA. [4]Department of Biochemistry, University of Wisconsin-Madison, Madison, WI, USA.
*Corresponding author. Email: jose.perez@csic.es

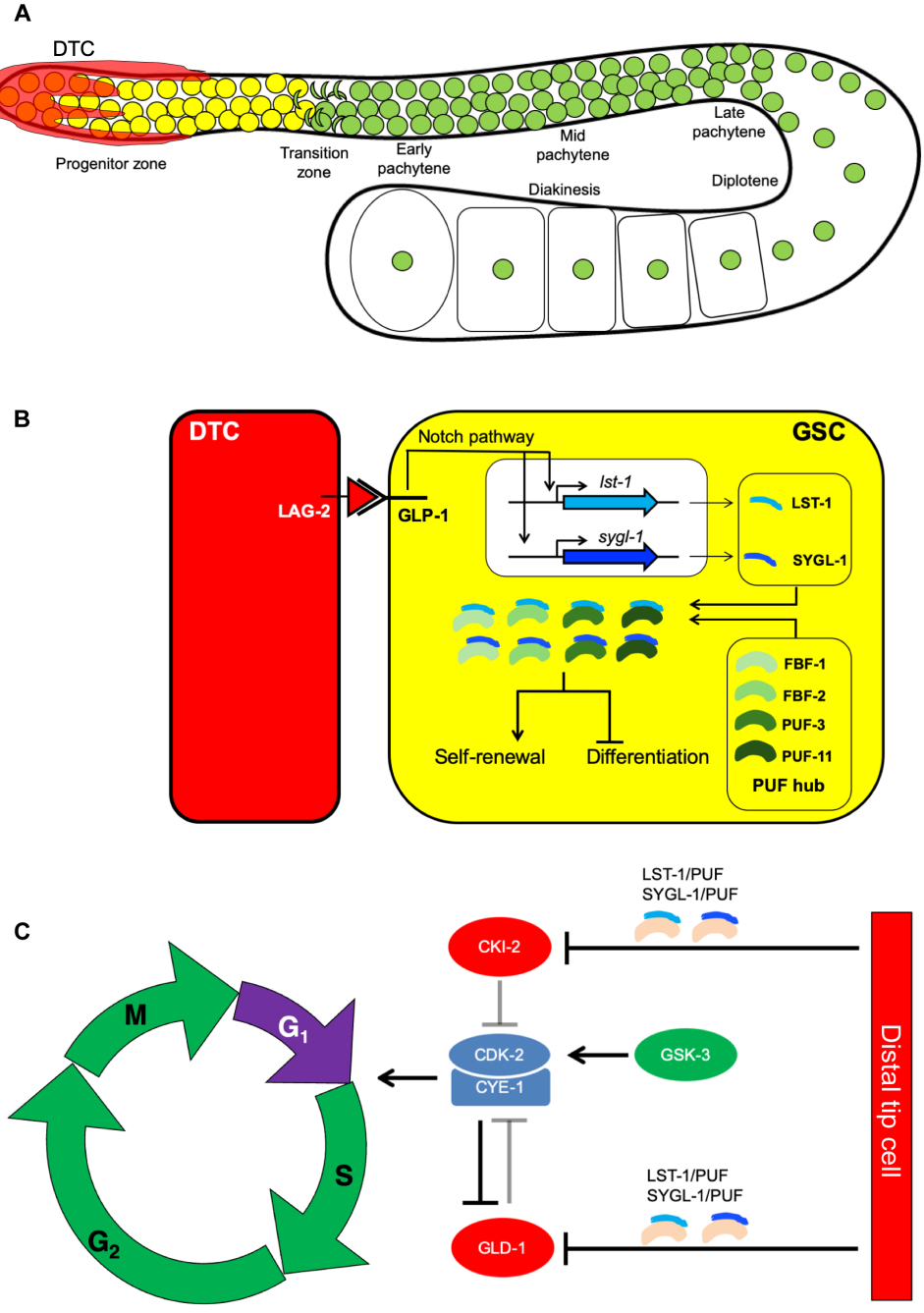

Fig. 1. The gonad from *C. elegans* and its regulation. (**A**) Diagram illustrating the gonad of a *C. elegans* hermaphrodite. The DTC (red) caps the distal end of the gonad and covers the germline PZ, which contains GSCs (yellow circles). The TZ is shown by crescent-shaped forms corresponding to cells in early meiotic prophase (zygotene, diplotene). Green circles represent germ cells at later stages of the meiotic cell cycle. (**B**) The DTC promotes GSC stemness through GLP-1/Notch signaling, which activates transcription of *lst-1* and *sygl-1*. The LST-1 and SYGL-1 proteins form a central regulatory hub as partners with four PUF proteins. PUF/LST-1 and PUF/SYGL-1 heterodimers repress differentiation-promoting RNAs, thereby maintaining stemness in the GSC pool. (**C**) DTC signaling acts through PUF hub partnerships to enhances activity of the S-phase CDK complex, resulting in a shortened G_1 phase within the GSC pool.

provides a structural scaffold for the widely conserved polycomb repressive complex 2 (PRC2), which drives histone methylation and produces repressive H3K27me3 (*15*, *16*). MES-4 is a histone methyltransferase that produces H3K36me3, a marker of actively transcribed genes (*17*, *18*). The loss of MES-4 or MES-3 results in the early differentiation of germ cells, which led to the view that MES-4 and PRC2 facilitate expression of germline genes while suppressing the expression of somatic genes in the germ line (*19*). However, recent studies support a model in which MES-4 and PRC2 promote germline survival and proliferation by silencing an oogenesis program that interferes with the fate of nascent germ cells (*20*–*22*). Despite extensive investigation into the role of these chromatin

modifiers, its regulatory relationship with the niche remains unclear. The drop of cellular MES-3 levels in the early pachytene stage has been attributed to GLD-1–mediated translational repression via the *mes-3* 3′ untranslated region (3′UTR and therefore indirectly regulated by the Notch pathway (*14*). We aimed to characterize the mechanisms underlying the substantial down-regulation of MES-4 and MES-3 expression upon meiotic entry to investigate whether the niche regulates the levels of these chromatin regulators in the gonads.

In this study, we report that the anaphase-promoting complex/cyclosome (APC/C) complex and its activator Fzr1/Cdh1 (APC/$C^{Fzr1/Cdh1}$) facilitate degradation of the proteins MES-4 and MES-3 in cells as they reach the TZ. APC/$C^{Fzr1/Cdh1}$ is a multisubunit E3 ubiquitin ligase that polyubiquitinates target proteins, leading to their degradation by the proteasome. While APC/$C^{Fzr1/Cdh1}$ is well-known for its role in regulating the cell cycle (*23*), its functions in development remain less studied (*24*). Here, we report that Notch signaling from the niche regulates APC/$C^{Fzr1/Cdh1}$ in the distal gonad, offering a potential mechanism by which the niche modulates levels of MES-4 and MES-3 in *C. elegans* gonads.

RESULTS

APC/C^{FZR-1} controls MES-4 levels in the gonad

The absence of MES-3 in the early pachytene stage has been attributed to translational repression directed by its 3′UTR (*14*). The reduction in protein levels in cells entering pachytene has been noted for other germline proteins that are regulated post-transcriptionally through their 3′UTRs (*25*). To investigate whether a similar mechanism operates for MES-4, we constructed a *mes-4* allele tagged with green fluorescent protein (GFP) at its endogenous locus, including its native 3′UTR, which accurately reflects the distribution of native MES-4 protein in the germ line (fig. S1). We then compared the expression of this allele with similar constructs in which we replaced the native 3′UTR with two heterologous 3′UTR regions from ubiquitously expressed genes, specifically *let-858* and *tbb-2*. The distribution of MES-4::GFP along the length of the gonad was similar regardless of its 3′UTR (Fig. 2A). Although we cannot rule out that the distribution may be regulated by mRNA sequences outside the 3′UTR (*26*), we sought to explore other possible mechanisms.

Proteasome activity regulates the decision between proliferation and meiotic entry in the *C. elegans* germ line (*27*). To determine whether the proteasome is involved in the decrease of MES-4 levels, we used RNA interference (RNAi) to silence *pas-4* and *pbs-5*, which encode the α and β subunits of the proteasome, respectively (*28*). MES-4::GFP became evenly distributed in the germ line upon proteasome down-regulation (Fig. 2B), suggesting that the MES-4 decrease relies on protein degradation. Among ubiquitin complexes that promote protein degradation in the gonads, the RING finger ubiquitin ligase RFP-1 and Skp, Cullin, F-box containing (SCF) complex associated with the F-box protein PROM-1 act in the distal gonad (*9*, *29*, *30*). However, the MES-4::GFP germline distribution was not altered by RNAi depletion of *rfp-1* or *prom-1* (fig. S2). The analysis of the MES-4 amino acid sequence revealed a KEN box with a high score (fig. S3). The KEN box is typical of proteins targeted for degradation by the E3 ubiquitin ligase APC/C. Strikingly, the MES-4::GFP distribution in the gonad became uniform after RNAi against *emb-27*, which encodes a core APC/C subunit (Fig. 2C) (*31*).

APC/C function relies on interactions with its activators, Cdc20 and Cdh1/Fzr1 [FZY-1 and FZR-1, respectively, in *C. elegans* (*32*, *33*)], to bring substrates to the catalytic core. Silencing *fzr-1* using RNAi resulted in MES-4::GFP expression throughout the germ line, while silencing *fzy-1* did not affect the distribution of MES-4::GFP (Fig. 2C). A similar uniform distribution was observed for MES-4::GFP when we introduced *mes-4::gfp* into worms carrying the hypomorphic *fzr-1*(*ku298*) allele (Fig. 2D) (*32*). This result was not attributable to the GFP tag, as it was also observed by immunostaining of untagged MES-4 worms after *fzr-1* RNAi (fig. S4). To further test the hypothesis that APC/C^{FZR-1} targets MES-4 for degradation, we mutated its KEN box by substituting key amino acids with alanine residues to create the *mes-4*^{AAA}*::gfp* allele. Similar to the MES-4 distribution in *fzr-1* (*ku298*), MES-4^{AAA}::GFP distribution was uniform (Fig. 2D). We concluded that APC/C^{FZR-1} promotes MES-4 degradation upon meiotic entry (Fig. 2E).

APC/C^{FZR-1} and the *mes-3* 3′UTR both regulate MES-3 levels

We also found a KEN box in the MES-3 amino acid sequence (fig. S3), which prompted us to analyze the distribution of a MES-3::GFP fusion protein in the gonads of *fzr-1*(*ku298*) mutants. Our findings suggested that APC/C^{FZR-1} regulates the MES-3 distribution along the gonad (Fig. 3A). The substitution of amino acids in the KEN box with alanine residues at the *mes-3* locus (*mes-3*^{AAA}) yielded similar results (Fig. 3A). However, disabling the proposed APC/C^{FZR-1}-mediated degradation of MES-3 did not fully abolish the decrease in MES-3 levels in cells entering meiosis (Fig. 3A).

The absence of MES-3 at the early pachytene stage has been attributed to translational repression via its 3′UTR (*14*). Thus, we investigated whether the inhibition of *mes-3* mRNA translation and the APC/C^{FZR-1}-promoted degradation of MES-3 protein operate together to reduce MES-3 levels in meiotic but not in mitotic germ cells. To this end, we constructed worm strains carrying the endogenous *mes-3::gfp* or *mes-3*^{AAA}*::gfp* alleles in which we replaced the native 3′UTR with that from *tbb-2*, a ubiquitously expressed gene that is not repressed by GLD-1 (*34*). Unexpectedly, the replacement of the 3′UTR region decreased MES-3 levels in the distal-most region in both cases (fig. S5A). To rule out potential unspecific effects of the *tbb-2* 3′UTR, we replaced the *mes-3* 3′UTR in the *mes-3::gfp* allele with two other alternative 3′UTRs from *let-858* and *mes-6* (another PRC2 subunit, also expressed in gonads); similar results were obtained (fig. S5B). These results suggest that sequences in the *mes-3* 3′UTR facilitate the translation of the *mes-3* mRNA in the distal region in a manner that cannot be fulfilled by other 3′UTRs. Nevertheless, we readjusted the fluorescence levels in each gonad (Fig. 3B) to measure relative fluorescence along the gonad in the four different GFP-tagged alleles: *mes-3*, *mes-3*^{AAA}, *mes-3 tbb-2 3′UTR*, and *mes-3*^{AAA} *tbb-2 3′UTR* (considering 100% of intensity the highest fluorescence value for each individual gonad from the distal tip to the late pachytene region, ~80% of the distance from the tip to the bend). We then compared the distribution of MES-3::GFP fluorescence along the length of the gonad for each allele. Replacing the 3′UTR reduces, although does not eliminate, the decrease in the fluorescence signal when cells enter the meiotic phase. However, when the 3′UTR is replaced and the KEN box is mutated in a single allele, the fluorescence signal is uniformly distributed along the length of the gonad (Fig. 3B). These results are consistent with the hypothesis that the APC/C^{FZR-1} and the *mes-3* 3′UTR cooperate to decrease MES-3 levels in meiotic germ cells (Fig. 3C). In summary,

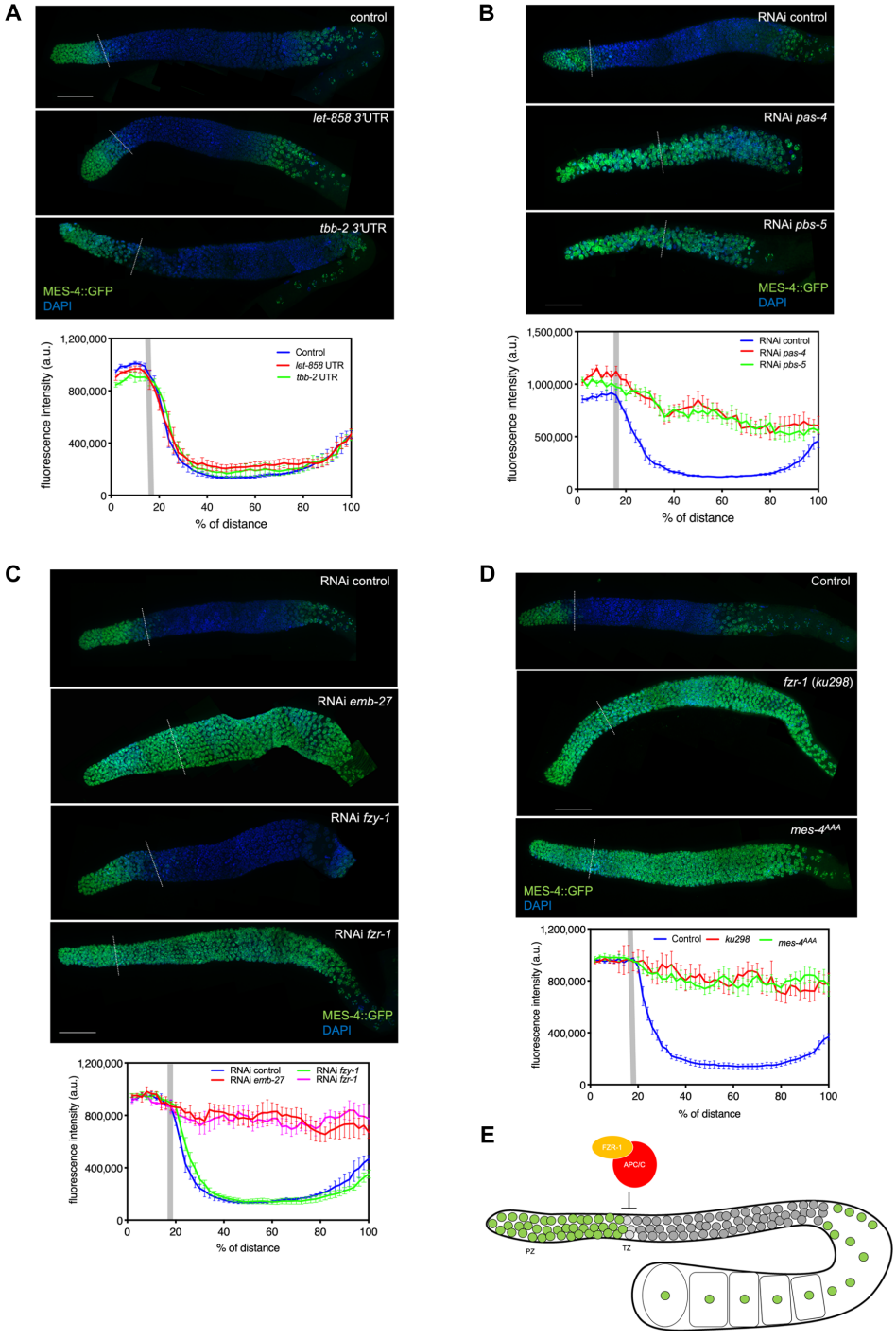

Fig. 2. APC/C^{FZR-1} controls MES-4 distribution along length of the gonad. (**A** to **D**) Top: images of young adult (1-day) dissected gonads, stained for DAPI (blue) and GFP (green); dashed line marks PZ/TZ boundary, recognized by morphology of 4′,6-diamidino-2-phenylindole (DAPI)–stained nuclei. In all images, scale bar: 50 μm. Bottom: Quantitation of GFP signal along length of gonad. Each line shows average GFP intensity ± SEM measured in arbitrary units (five gonads each). The *x* axis represents relative distance along gonads from the most distal end to the bend. Gray bar indicates location of the average localization of PZ/TZ boundary. (A) *mes-4* 3′UTR has minimal effect on MES-4 protein distribution. Gonads from worms carrying *mes-4::gfp* allele (control) and variants in which the native 3′UTR was exchanged with the indicated 3′UTR. (B) Silencing the proteasome extends MES-4 signal through pachytene. Gonads from worms carrying *mes-4::gfp* allele and silenced for two genes encoding proteasome components (*pas-4* and *pbs-5*). (C) Silencing APC/C changes MES-4 distribution. Images show gonads from worms carrying the *mes-4::gfp* allele and silenced for genes encoding APC/C core component Apc6 (*emb-27*) and activators Cdc20 (*fzy-1*) and Cdh1/Fzr1 (*fzr-1*). (D) APC/C^{FZR-1} targets MES-4 for degradation. Gonads from worms carrying *mes-4::gfp* allele in a wild-type or *fzr-1*(*ku298*) background. Gonad from a worm carrying the *mes-4^{AAA}::gfp* allele is also shown. (**E**) Summary diagram. Germ cells expressing MES-4 are highlighted in green; those without MES-4 are in gray. APC/C^{FZR-1} facilitates MES-4 degradation as cells enter the TZ.

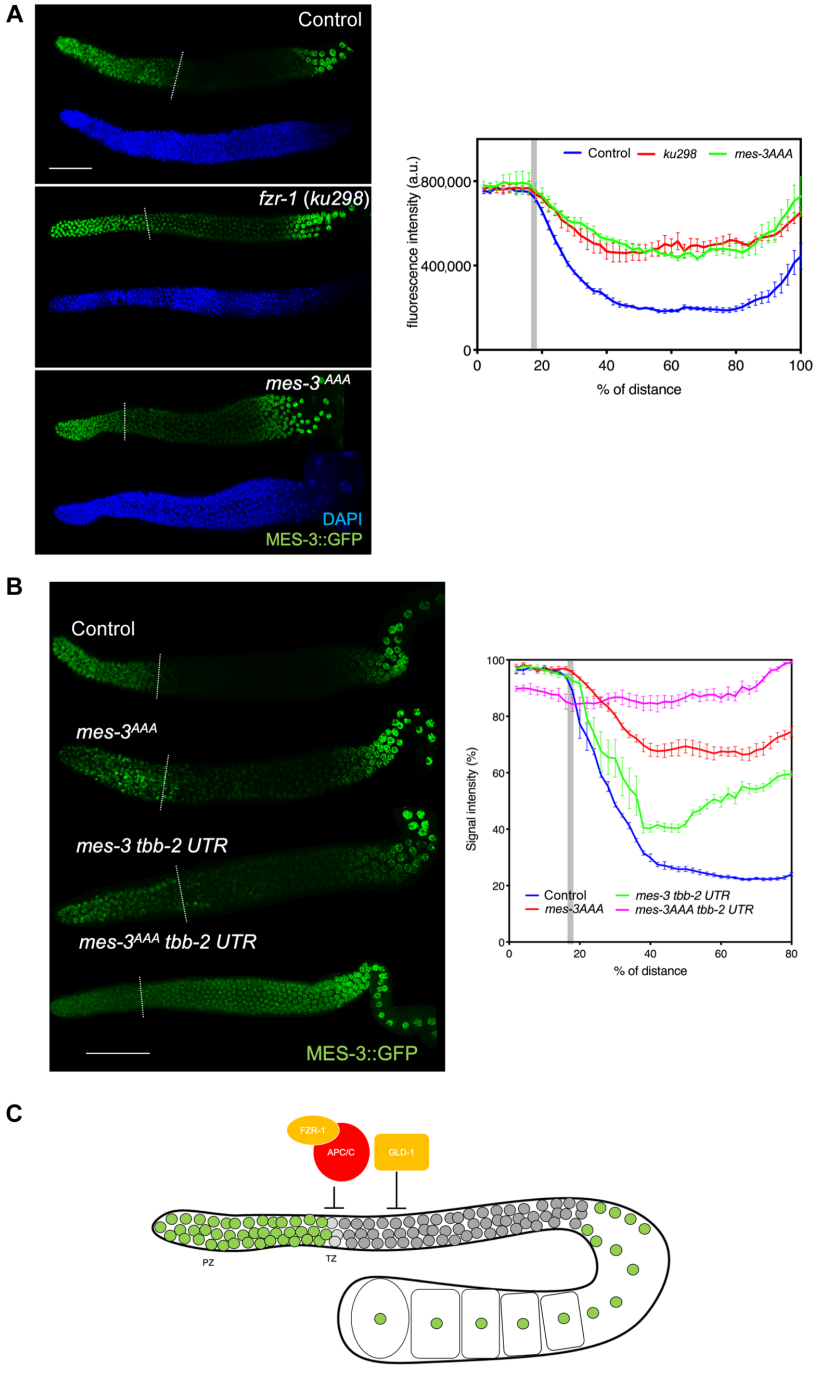

Fig. 3. Both APC/C^{FZR-1} and *mes-3* 3′UTR regulate MES-3 protein the distribution along length of the gonad. (**A** and **B**) Left panels show images of young adult (1-day) dissected gonads, stained for DAPI (blue) and GFP (green); dashed line marks PZ/TZ boundary, recognized by morphology of DAPI-stained nuclei. In all images, scale bar: 50 μm. The right panels show quantitation of GFP signal along length of gonad. Gray bar indicates location of the average localization of PZ/TZ boundary. (A) APC/C^{FZR-1} targets MES-3 protein for degradation. The gonads were extracted from worms carrying the *mes-3::gfp* allele in a wild-type (control) or *fzr-1*(*ku298*) background. A gonad from a worm carrying the *mes-3^{AAA}::gfp* allele is also shown. The right panel shows average GFP intensity ± SEM measured in arbitrary units (five gonads each). The *x* axis represents relative distance along gonads from the most distal end to the bend. (B) The 3′UTR collaborates with APC/C^{FZR-1} to regulate MES-3 distribution in the gonad. Gonads were extracted from worms carrying different *mes-3::gfp* alleles: *mes-3* (control); *mes-3^{AAA}* carrying the KEN to AAA; *mes-3 tbb-2* 3′UTR in which the native *mes-3* 3′UTR was replaced by the *tbb-2* 3′UTR; and *mes-3^{AAA} tbb-2* 3′UTR carrying both changes. The fluorescence intensity images from gonads carrying the *tbb-2* 3′UTR were enhanced (see fig. S5A for unenhanced images). The right panel shows the relative levels of MES-3::GFP along the gonad. Relative values were adjusted to the maximum fluorescence intensity in each gonad (seven gonads in total). The graph line shows the average relative GFP intensity ± SEM. (**C**) Summary diagram. Germ cells expressing MES-3 are highlighted in green; those without MES-3 are in gray. APC/C^{FZR-1} facilitates MES-3 degradation as cells enter the TZ, while the action of GLD-1 represses translation of *mes-3* mRNA once cells enter the meiotic cell cycle.

we found evidence strongly suggesting that the E3 ubiquitin-ligase complex APC/C^{FZR-1} is involved in the decrease of MES-4 and MES-3 levels in cells as they transition from the mitotic to meiotic region in the gonad of *C. elegans*.

FBF proteins and APC/C^{FZR-1} regulate FZR-1 levels in the distal gonad

As MES-4 and MES-3 are both enriched in the distal mitotic nuclei in the germ line, we hypothesized that FZR-1 would be absent or only present at low levels in the mitotic region. Thus, we tagged FZR-1 with the V5 epitope at its N terminus and analyzed germ lines carrying *v5::fzr-1* and *mes-4::gfp* alleles. Quantification of the normalized V5-associated signal intensity revealed low levels of FZR-1 in the distal-most part of the germ line. These levels increased as cells approached the TZ, where they reached a maximum and abruptly dropped when cells entered pachytene (Fig. 4A). We confirmed this distribution pattern by observing unfixed gonads using an N-terminal-tagged *gfp::fzr-1* allele (fig. S6).

Consistent with the proposed role of APC/C^{FZR-1} in facilitating MES-4 degradation, we observed that as FZR-1 levels peaked, the levels of MES-4::GFP began to decrease, indicating a correlative relationship (Fig. 4A). Notably, the decline in FZR-1 levels was closely aligned with the MES-4 decrease. The sudden drop in FZR-1 levels in cells transitioning into meiosis resembled the APC/C-mediated self-degradation of Cdh1 observed in yeast meiotic cells (*35*). To explore this hypothesis, we silenced *emb-27*, a subunit of APC/C, and analyzed GFP::FZR-1 levels in gonads. Our results showed a considerable increase in the GFP fluorescence signal in the pachytene region (fig. S7A), strongly suggesting that APC/C mediates the decrease of FZR-1 levels. Silencing of *fzy-1* (Cdc20 in mammals) did not replicate the GFP::FZR-1–induced pachytene invasion observed when *emb-27* was silenced (fig. S7A). This suggests that FZR-1 mediated its degradation. The FZR-1 amino acid sequence contains a putative destruction box (D-box) near the N terminus (figs. S3 and S7B). Mutating critical residues of the D-box to alanine (*fzr-1^{db}* allele) resulted in the stabilization and presence of FZR-1 throughout the germline (fig. S7C). On the basis of these results, we propose that APC/C^{FZR-1} recognizes FZR-1 and promotes its self-degradation via the D-box motif, resulting in the absence of FZR-1 in pachytene.

We also investigated the mechanisms involved in maintaining low levels of FZR-1 in the distal-most part of the gonad. We analyzed the activity of the *fzr-1* promoter using a transcriptional GFP::H2B fusion. GFP levels increased as the cells approached the meiotic region, although a measurable signal was present in the mitotic region (fig. S8). This suggests that some posttranscriptional control over *fzr-1* must exist to maintain low FZR-1 levels in the distal-most part of the gonad.

The 3′UTR region of *fzr-1* binds the translational repressors FBF-1 and FBF-2 (*36*). Because these repressors are more active in the most distal region of the gonad, we hypothesized that FBF activity could regulate FZR-1 levels. Using a strain carrying the *v5::fzr-1* allele, we investigated whether the FZR-1 levels were affected by down-regulation of FBF expression using RNAi directed against the *fbf-1/2* genes. FZR-1 levels markedly increased in the mitotic region of the germ line in response to silencing FBF (Fig. 4B). We further created an *fzr-1* 3′UTR reporter consisting of the *pie-1* promoter that transcribes a GFP::H2B fusion and the 3′UTR from *fzr-1* (*25*). The *fzr-1* 3′UTR reporter and a control carrying the 3′UTR from *tbb-2* were inserted as a single copy using the Mos system. The 3′UTR from *fzr-1* caused low expression of the reporter in the PZ (Fig. 4C). However, RNAi against *fbf-1/2* attenuated down-regulation of the GFP signal in the distal-most part of the gonad, suggesting that FBF proteins down-regulate FZR-1 via the *fzr-1* 3′UTR.

These results provide a framework for explaining the FZR-1 distribution in the distal gonad. The limited transcriptional activity of the *fzr-1* promoter and the repressor activity of FBF proteins result in low FZR-1 levels in the region close to the distal tip, but these levels increase as germ cells reached the TZ. This pattern most likely results from increased transcriptional activity and decreased FBF-mediated repression. Once cells enter the meiotic cell cycle, the APC/C^{FZR-1} complex is activated (or derepressed, see below), and its targets, including FZR-1, are consequently degraded by the proteasome.

We examined the consequences of disabling the proposed regulatory framework. Our first focus was on the effects of turning off FZR-1 self-degradation. The *fzr-1^{db}* allele, which could not be targeted by APC/C, functions comparably to the wild-type allele, at least in terms of promoting MES-4 degradation (fig. S9A). However, worms carrying the *fzr-1^{db}* allele experience significant fertility issues (fig. S9B), mainly due to a reduced number of embryos (fig. S9C). Although we cannot exclude somatic effects, abnormally enlarged oocytes were seen in gonads derived from *fzr-1^{db}* mutants (fig. S9D). The sustained presence of FZR-1 in the pachytene region of these mutant worms may result in the unscheduled degradation of proteins important for oocyte development.

We further sought to determine the importance of maintaining low levels of FZR-1 in the mitotic region for the regulation of APC/C^{FZR-1} activity. To this end, we analyzed the levels of MES-4::GFP (as a readout of APC/C^{FZR-1} activity) under conditions that enable accumulation of FZR-1 in the most distal gonad. In control gonads, signal from MES-4::GFP extended to 30 gcd from the distal tip of the germ line on average. In *fbf-1/2*–silenced gonads (conditions in which we observed a dramatic increase in FZR-1 expression in the distal gonad), MES-4::GFP signal extended to 24 gcd on average (Fig. 4D). This result suggests that high levels of FZR-1 in the mitotic region accelerate MES-4 down-regulation. However, the absence of a stronger effect (e.g., MES-4 degradation along the entire distal region) suggests the presence of additional ways to restrict APC/C^{FZR-1} activity in the mitotic region, besides regulation of FZR-1 levels. In summary, we found that FBFs work together with APC/C^{FZR-1} to control the distribution and levels of FZR-1 in the germ line (Fig. 4E).

CDK activity prevents APC/C^{FZR-1} activity in the mitotic region of the gonad

We sought to elucidate the additional mechanisms underlying APC/C^{FZR-1} regulation along the most distal part of the gonad. The interaction between Cdh1/Fzr1 and the APC/C core is negatively regulated by phosphorylation of Cdh1/Fzr1 by the CDK complex at several sites (*37*). CDK-mediated inhibitory phosphorylation appears to be widely conserved, including in yeast, *Drosophila,* and mammalian cells [reviewed in (*38*)]. In vitro assays revealed that CDK complexes can phosphorylate FZR-1 in *C. elegans* (*39*). These phosphorylation sites are in conserved regions that are important for interactions with APC/C core subunits (fig. S10).

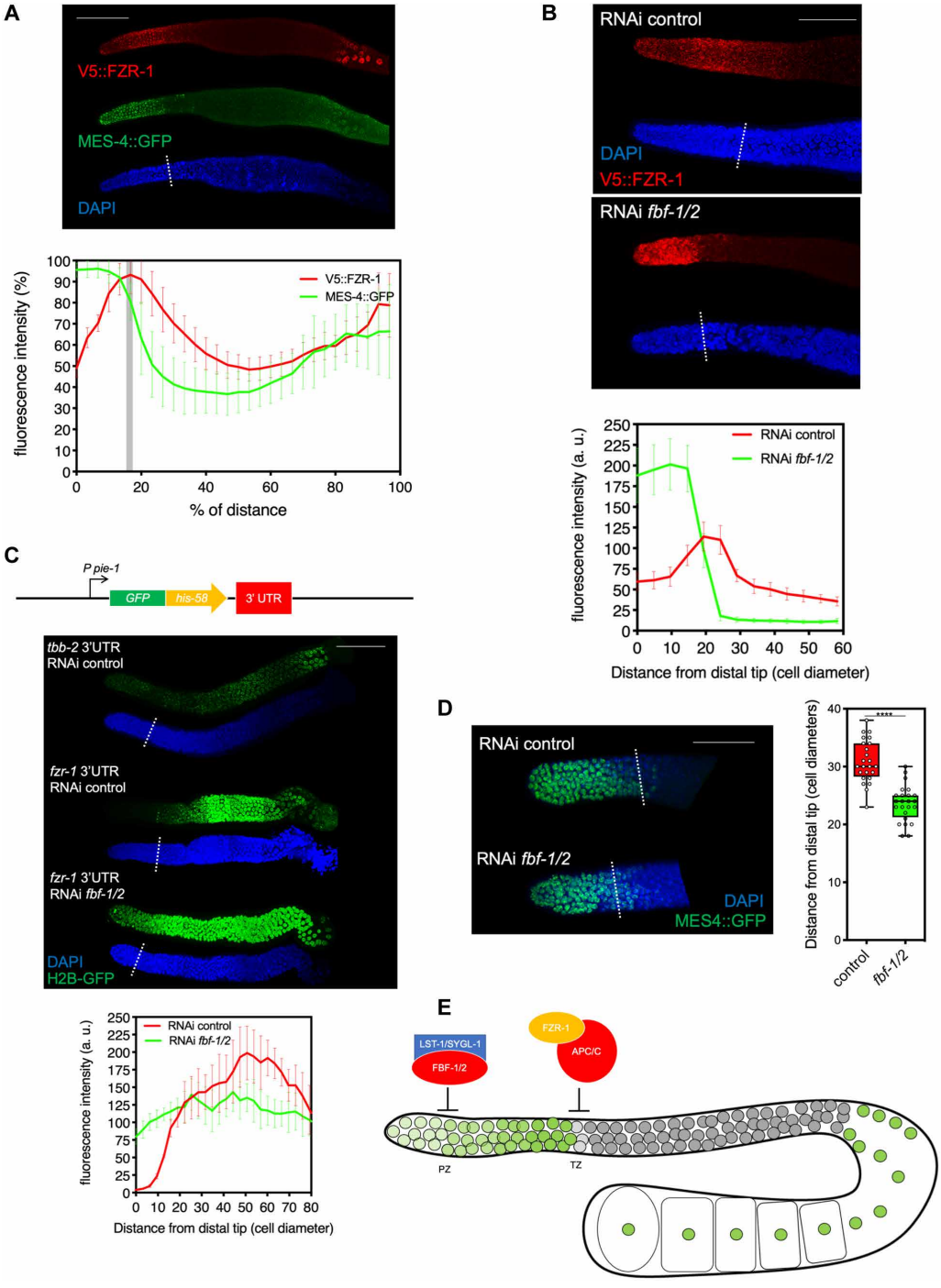

Fig. 4. FBF and APC/C regulate FZR-1 levels. (**A** to **D**) Images of young adult (1-day) dissected gonads. Dashed line marks PZ/TZ boundary, recognized by morphology of DAPI-stained nuclei. In all images, scale bar: 50 μm. (A) Comparison of FZR-1 and MES-4 levels. Gonad arms were dissected from worms carrying tagged versions of FZR-1 (V5::FZR-1) and MES-4 (MES-4::GFP) stained with anti-V5 (red), anti-GFP (green), and DAPI. The graph shows the relative levels of each protein adjusted to the maximum fluorescence intensity in each gonad and for each protein (13 gonads in total). (B) FBF regulates FZR-1 expression at the distal part of the gonad. Gonad arms were dissected from worms carrying the *V5::fzr-1* allele silenced with a control RNAi (pL4440) or *fbf-1/2* RNAi, stained with anti-V5 antibody and DAPI. The graph shows the relative levels of V5::FZR-1 along the gonad measured as germline cell diameters from the distal tip (13 gonads each). (C) *fzr-1* 3′UTR mediates repression in the distal part of the gonad. Images of gonads from worms carrying the reporter controlled by the indicated 3′UTRs are shown. The graph shows the relative levels of GFP-associated fluorescence along the gonad measured as germline cell diameters from the distal tip. Each line shows the average fluorescence intensity ± SEM measured in arbitrary units (five gonads each). (D) FBF regulates APC/C^{FZR-1} activity in the distal gonad. Images of the distal region from gonads dissected from worms carrying the *mes-4::gfp* allele in control or *fbf-1/2* silenced conditions. The graph shows distance, in germline cell diameters, between the distal tip of the germline and the end row of continuous MES-4::GFP accumulating cells from 24 gonads in each condition. $P < 1 \times 10^{-4}$. (**E**) Summary diagram. Germ cells expressing FZR-1 are highlighted in green (intensity reflects protein amounts), and those without FZR-1 are in gray.

We investigated whether high CDK activity in the PZ (*9*) could be responsible for the hypothesized down-regulation of APC/C^{FZR-1} activity in the most distal gonad in *C. elegans*. To this end, we analyzed whether MES-4::GFP was prematurely degraded in gonads depleted through RNAi of the components of various cell cycle–related CDK complexes in *C. elegans*: the CDK4 complex (*cdk-4* and *cyd-1*), CDK2 (*cdk-2*, *cye-1* and *cya-1*), and CDK1 (*cdk-1*, *cyb-1* and *cyb-3*) [reviewed in (*40*)] (Fig. 5, A and B). The most considerable effect was observed upon the silencing of *cdk-2* or its partner *cye-1*; the MES-4::GFP signal was fainter and limited to the most distal part of the gonad, extending, on average, between 5 and 8 gcd (Fig. 5C).

We silenced *cye-1* in a strain carrying the *mes-4^{AAA}* allele tagged with GFP to determine whether the decrease in MES-4::GFP levels was due to effects of the down-regulation of CDK activity unrelated to APC/C^{FZR-1} activity such as the decrease in the transcriptional expression of *mes-4*. MES-4^{AAA} was not prematurely degraded following *cye-1* silencing (fig. S11). This result strongly links the decrease in CDK activity to an increase in APC/C^{FZR-1} activity. We suggest therefore that the CYE-1/CDK-2 complex may be mainly responsible for down-regulation of APC/C^{FZR-1} activity in the distal gonad (Fig. 5D).

We further sought to confirm whether CDK negatively regulates the activity of APC/C^{FZR-1} via the inhibitory phosphorylation of FZR-1 in the mitotic region of the gonad. To this end, we constructed a mutant *fzr-1* allele (*fzr-1^{9A}*) carrying alanine substitutions in the described in vitro CDK phosphorylation sites (eight sites) and one putative conserved phosphorylation site (fig. S10) (*41*). All attempts to insert the *fzr-1^{9A}* allele into worms as an ectopic copy were unsuccessful (contrary to the wild-type version of the same construction), suggesting that the mutant allele was deleterious. To circumvent this technical problem, we constructed a version of the mutant allele in which an intervening sequence (consisting of a hygromycin resistance gene) flanked by *lox* target sites of Cre recombinase was inserted between the promoter and the open reading frame of the mutant allele. Cre-induced recombination resulted in the excision of the intervening sequence and the expression of the mutant allele (Fig. 6A). This construct was inserted on chromosome IV using the Mos system. To induce recombination, the Cre recombinase was generated by crossing hermaphrodites with males carrying a transgene expressing Cre recombinase in the germ line (Fig. 6B). We analyzed the gonads from the progeny (1-day-old adults) resulting from crosses of hermaphrodite worms carrying the *mes-4::gfp* allele and the corresponding ectopic *fzr-1* allele (wild type or *fzr-1^{9A}*) with males carrying the *mes-4::gfp* allele and the transgene providing Cre recombinase. Although expression of an ectopic copy of wild-type *fzr-1* did not seem to affect the distribution of MES-4::GFP-associated signals, the expression of *fzr-1^{9A}* resulted in absence of detectable MES-4. A clear and uniform fluorescent signal was observed when using the *mes-4^{AAA}::gfp* allele, which is refractory to APC/C^{FZR-1} promoted degradation (Fig. 6C). None of the hermaphrodites obtained from crosses with the nonphosphorylatable version of FZR-1 was fertile (Fig. 6D), and analysis of their gonads showed an aberrant morphology (Fig. 6E). The lack of fertility was not suppressed by the presence of nondegradable versions of MES-4 and MES-3 (Fig. 6D). This suggests that additional targets of APC/C^{FZR-1} are important for germline maintenance.

We investigated whether the presence of two distinct mechanisms that maintain APC/C^{FZR-1} inactivity in the mitotic region (e.g., the CDK-mediated inhibition of FZR-1 and the control of FZR-1 levels exerted mainly by FBF proteins) indicated collaborative functions. To this end, we quantified MES-4::GFP levels in worms in which *cye-1*, *fbf-1/2*, or both genes were silenced using RNAi. We observed an additive effect on the decrease of MES-4 levels when both negative regulatory circuits were simultaneously disabled (fig. S12). These results support the notion that at least two mechanisms collaborate to restrict APC/C^{FZR-1} activity in the mitotic region of the germ line (Fig. 5D).

SCF^{PROM-1} and APC/C^{FZR-1} cooperate in CYE-1 degradation and contribute to APC/C^{FZR-1} activation, together with additional regulators

Negative regulation of APC/C^{FZR-1} enables accumulation of MES-4, MES-3, and other unknown targets in the mitotic region of the germ line. However, this negative regulation must be alleviated as mitotic germ cells reach the TZ to allow timely activation of APC/C^{FZR-1} and subsequent degradation of its targets. CYE-1 levels remain high throughout the mitotic cell cycle but sharply decrease as germ cells enter meiosis (*9*). Thus, we hypothesized that the diminished CYE-1/CDK-2 activity at the end of the mitotic zone, caused by low CYE-1 levels, combined with an increase in FZR-1 production, results in the presence of nonphosphorylated FZR-1 that can bind to the APC/C core. This hypothesis is consistent with the finding that CYE-1 levels decreased by a few cell diameters before MES-4 degradation (Fig. 7, A and B), suggesting a causal relationship. Thus, we aimed to measure APC/C^{FZR-1} activity (using MES-4 levels as a readout) under high CYE-1 levels along the entire gonad to confirm this causal relationship. The PROM-1 protein associated with the SCF E3 ubiquitin ligase complex mediates the degradation of CYE-1 when cells reach meiosis. However, additional factors are required for the complete decrease of cyclin levels (*9*, *30*). We previously observed that *prom-1* silencing did not affect the distribution of MES-4 along the gonads (fig. S2). However, when analyzing CYE-1 and MES-4 levels in the same gonads, we noticed that MES-4 degradation roughly overlapped with CYE-1 degradation following *prom-1* silencing (Fig. 7C). On the basis of this observation, we hypothesized that SCF^{PROM-1} acts as a first-wave degrader of CYE-1 and that second-wave degradation occurs later. As this coincides with a decrease in MES-4 levels, we hypothesized that this second-wave degrader might be APC/C^{FZR-1}. While the absence of FZR-1 or PROM-1 alone did not result in CYE-1::GFP expression throughout the pachytene region, the depletion of PROM-1 in *fzr-1 (ku298)* worms by RNAi resulted in the GFP signal being distributed throughout the germ line (Fig. 7D), indicating the redundant role of SCF^{PROM-1} and APC/C^{FZR-1} in the decrease of CYE-1 levels when germ cells reached meiosis. Consistent with these findings, the amino acid sequence of CYE-1 contains both KEN and destruction boxes (fig. S3). Thus, we constructed the *cye-1^{AAAdb}* allele by exchanging the amino acids comprising the KEN-box and D-box with alanine residues. The decrease of CYE-1 levels when the cells reached pachytene was disabled when the *cye-1$^{AAA\ db}$::gfp* allele was combined with *prom-1* silencing (Fig. 7D). In summary, SCF^{PROM-1} and APC/C^{FZR-1} appear to cooperate to decrease the CYE-1 levels once germ cells reach the TZ (Fig. 7E).

We maintained high CYE-1 levels along the gonads to evaluate MES-4::GFP levels as a readout of APC/C^{FZR-1} activity. To this end, *prom-1* was silenced in a strain carrying the *cye-1$^{AAA\ db}$* allele. Although MES-4 accumulated more proximally than in the control gonads, eventually its levels dropped (Fig. 7, F and G). This indicates

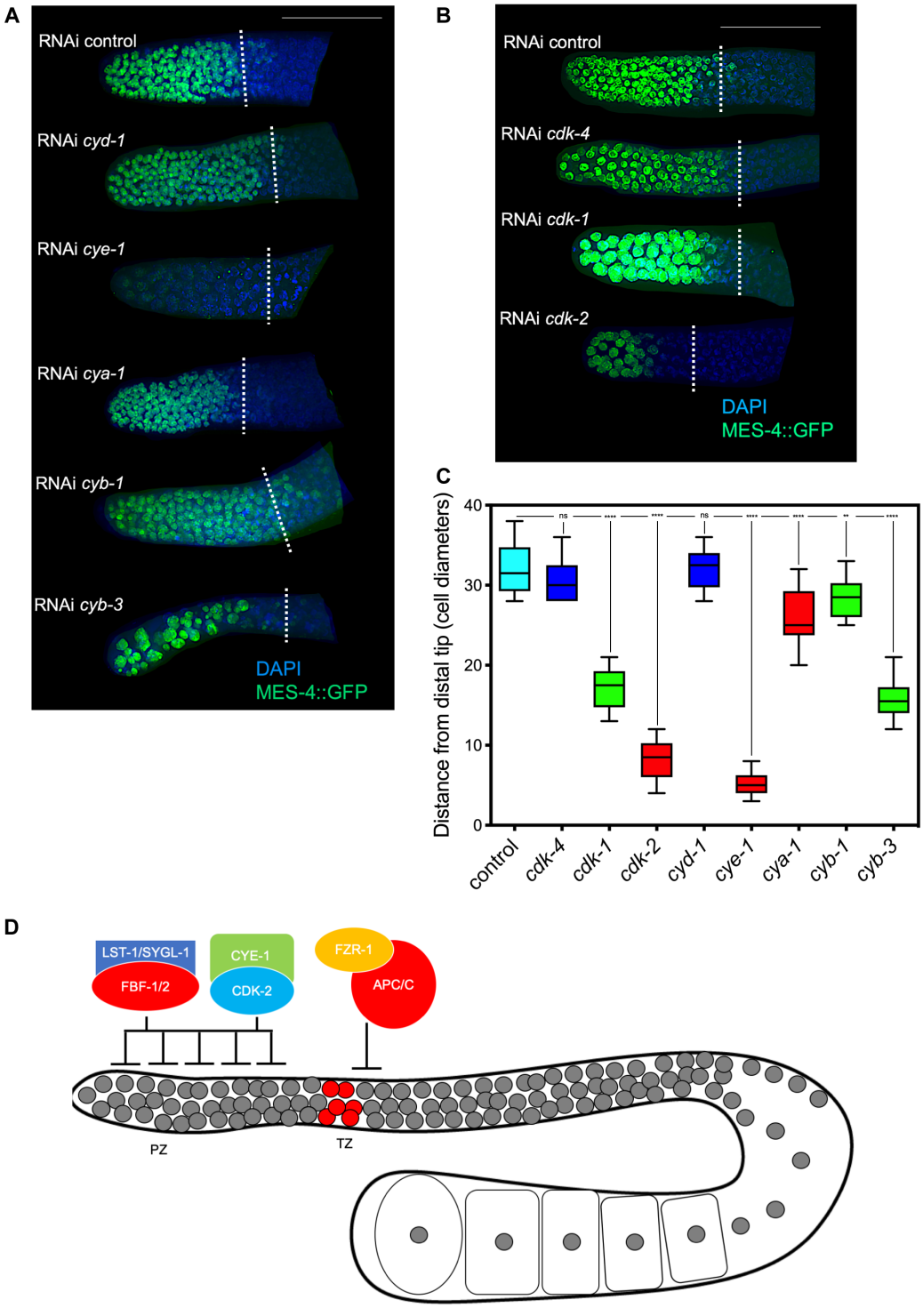

Fig. 5. CDK regulates APC/C^{FZR-1} activity in the PZ. (**A** and **B**) Images of distal region from gonads dissected from young adult (1-day) worms carrying the *mes-4::gfp* allele in control or distinct Cyclin-encoding (A) and Cdk-encoding (B) genes under silenced conditions. Dashed lines indicate the PZ/TZ boundary defined by the morphology of DAPI-stained nuclei. Scale bar, 50 μm. (**C**) Graph showing the distance, in germline cell diameters, between the distal tip of the germline and the end row of continuous MES-4::GFP-accumulating cells during RNAi silencing of the indicated genes. The different color boxes represent control RNAi (cyan), CDK1 complex (green), CDK2 complex (red), and CDK4 complex (blue), respectively (at least 10 gonads were measured for each condition). (**D**) Summary diagram of the results shown in Figs. 5 and 6, and figs. S7 and S12. Cells showing APC/C^{FZR-1} activity are highlighted in red. The collaborative action of FBF complexes and the CDK activity restricted the activity of APC/C^{FZR-1} in the PZ. This repression is released in the TZ, where the rise of APC/C^{FZR-1} activity promotes the degradation of FZR-1.

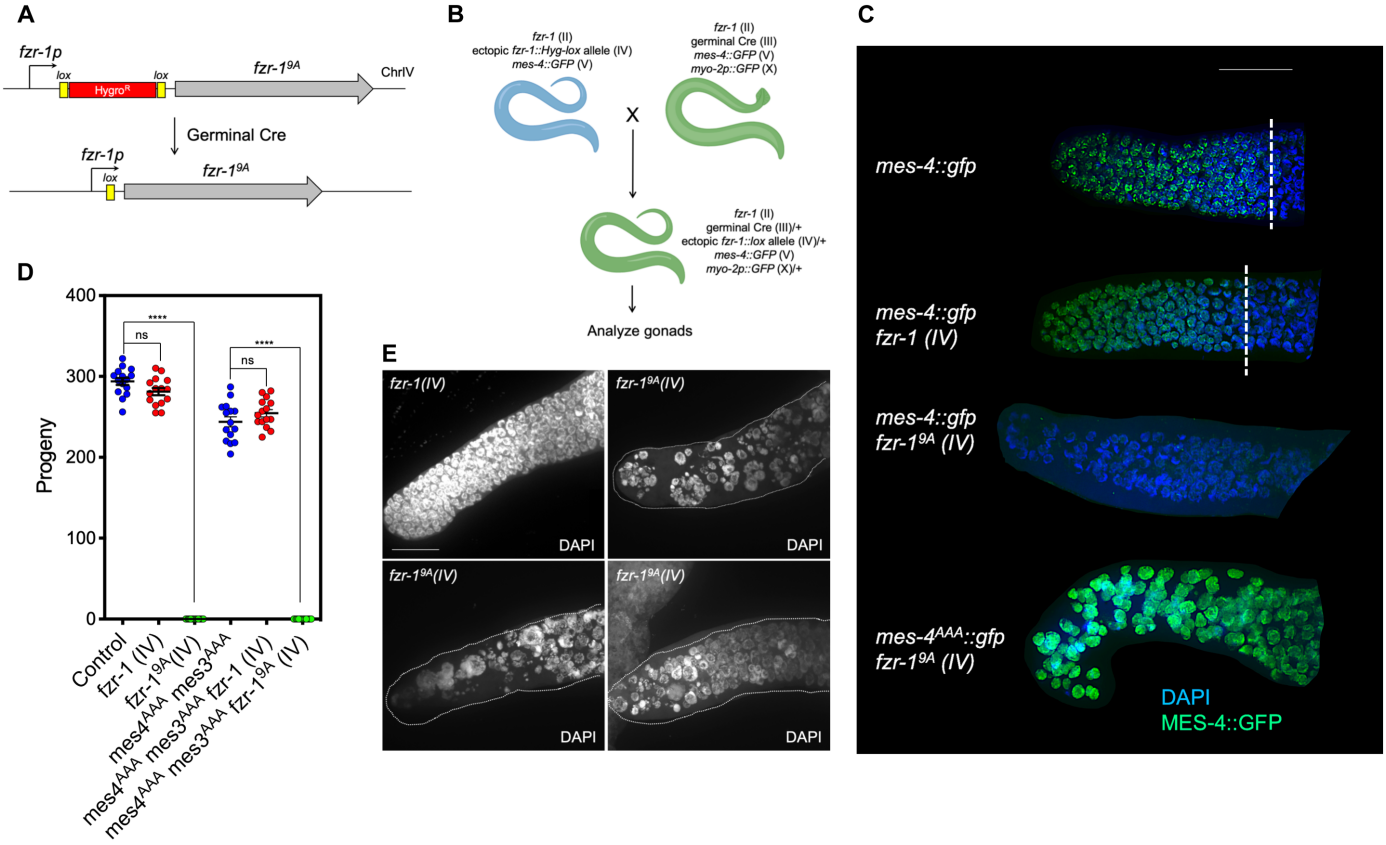

Fig. 6. Effects of an FZR-1 allele refractory to CDK-mediated phosphorylation. (**A**) Scheme depicting conditional Cre-dependent *fzr-1*^{9A} allele. The mutant and wild-type alleles were inserted at chromosome (Chr) IV using the Mos system. (**B**) Scheme showing cross leading to gonadal expression (upon Cre-mediated recombination) of the conditional *fzr-1*^{9A} allele. The *myo-2p::GFP* marker was used to sort hermaphrodite progeny originating from the cross. (**C**) Images of the distal region from gonads dissected from 1-day-old young adult hermaphrodites resulting from cross depicted in (B) carrying the indicated ectopic *fzr-1* (in Chr IV) and *mes-4::gfp* alleles. Dashed lines indicate the PZ/TZ boundary defined by the morphology of DAPI-stained nuclei. In gonads expressing *fzr-1*^{9A} allele, we could not detect a TZ. Scale bar, 50 μm. (**D**) Graph showing brood size of hermaphrodites obtained from crosses depicted in (C). ****$P < 1 \times 10^{-4}$; ns, not significant. (**E**) Images of the distal region of three dissected gonads stained with DAPI from 4-day-old adults resulting from cross of worms carrying conditional Cre-dependent *fzr-1*^{9A} allele and males carrying germline-expressed Cre. A control gonad resulting from cross of worms carrying the conditional Cre-dependent *fzr-1* allele and males carrying the germline-expressed Cre was included. Scale bar, 50 μm.

that APC/C^{FZR-1} was activated despite the high levels of CYE-1. This observation suggests that the decrease in the levels of CYE-1 is not the sole cause for the promotion of APC/C^{FZR1} activity and that additional factors may contribute to APC/C^{FZR-1} activation.

The CDK inhibitor CKI-2 contributes to the activation of APC/C^{FZR-1} in cells reaching meiosis

We sought to identify the additional elements involved in the timely activation (derepression) of APC/C^{FZR-1} in *C. elegans* gonads. One possibility could have been the presence in the PZ of APC/C inhibitors of the Emi1 family in mammals (*42*) or Rca1 in *Drosophila* (*43*), which could be removed when cells enter meiosis. We did not follow up on this option because no clear homologs have been identified in *C. elegans*. Furthermore, the marked effect seen in the analysis of the phosphorylation-refractory FZR-1^{9A} mutant suggests that the primary regulatory mechanism may be the inhibitory phosphorylation mediated by CDK. As a result, we shifted our focus to exploring alternative methods to control CDK activity.

During *Drosophila* development, the down-regulation of Cyclin E–Cdk2 expression before terminal divisions, in preparation for imminent cell cycle exit in differentiating cells, converts Cyclin A complexed to Cdk2 from a redundant into an indispensable negative regulator of APC/C^{Fzr} (*44*). We investigated whether CYA-1, a second partner of CDK-2, plays a similar role in the *C. elegans* gonad. The analysis of a GFP-tagged version of *cya-1* revealed that germ cells expressing CYA-1 were located at the edge of the region covered by the DTC processes (fig. S13A), a zone in which a small pool of cells complete the final mitotic cell cycle (*45*). We identified KEN and destruction boxes in the amino acid sequence of this protein (fig. S3). Furthermore, we confirmed that APC/C^{FZR-1} also targeted CYA-1 (fig. S13B). However, combining the stabilized *cya-1*$^{AAA\ db}$ and *cye-1*$^{AAA\ db}$ alleles with *prom-1* silencing did not lead to the expected uniform distribution of MES-4 along the gonad (Fig. 8A). Nonetheless, MES-4 accumulated more proximally than in control gonads (Fig. 8C), suggesting some degree of cooperation in maintaining APC/C^{FZR-1} inactivity between these two CDK complexes.

We further analyzed CKI-2 in this study. We hypothesized that APC/C^{FZR-1} was activated even under high levels of CYE-1 expression because the CDK-2/CYE-1 complex was repressed by other mechanisms. The *C. elegans* genome encodes two cyclin-dependent

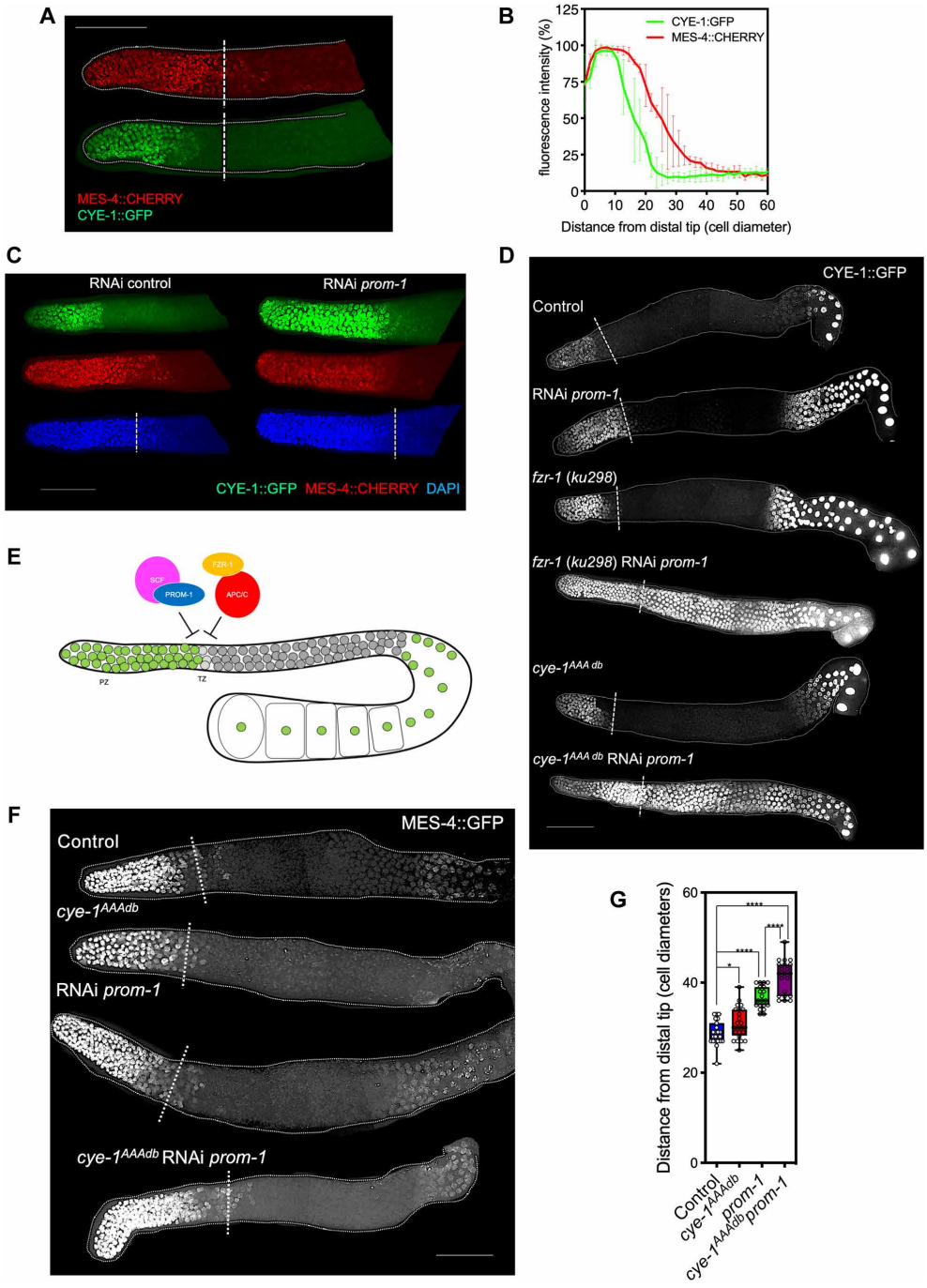

Fig. 7. Cooperative decrease of CYE-1 levels by SCF^{PROM-1} and APC/C^{FZR-1} is not enough to activate APC/C^{FZR-1}. (**A**, **C**, **D**, and **E**) Images of gonads dissected from young adult (1-day) worms. Dashed lines indicate the PZ/TZ boundary defined by the morphology of DAPI-stained nuclei. Scale bar, 50 μm. (A) Decrease of MES-4 precedes decrease in CYE-1. Distal region of gonad from a worm carrying *mes-4::cherry* and *cye-1::gfp* alleles. (**B**) Graph shows the quantification of GFP and Cherry intensity along the germ line from most distal in germline cell diameters in gonads from the worms described in (A). Each line shows the average fluorescent intensity ± SEM. Relative values were adjusted to the maximum fluorescence intensity for each fluorophore and in each gonad (four gonads in total). (C) CYE-1 and MES-4 levels are jointly decreased in the absence of PROM-1. Distal region of gonads from worms carrying *mes-4::cherry* and *cye-1::gfp* alleles and subject to RNAi control or *prom-1* RNAi. (D) SCF^{PROM-1} and APC/C^{FZR-1} promote the decrease of CYE-1 levels. Gonads from worms carrying the *cye-1::gfp* allele in the indicated genetic backgrounds or RNAi conditions. The allele *cye-1$^{AAA\ db}$* has the KEN and destruction boxes inactivated through point alanine substitutions of relevant residues. (E) Summary diagram. Cells expressing CYE-1 are highlighted in green. APC/C^{FZR-1} and SCF^{PROM-1} cooperate to facilitate the degradation of CYE-1 in cells reaching the TZ. (**F** and **G**) Decrease of CYE-1 levels is not solely responsible for the promotion of APC/C^{FZR-1} activity. Gonads from worms carrying the *mes-4::gfp* allele in the indicated genetic backgrounds or RNAi conditions and quantification of the distance (in germline cell diameters) between the distal tip of the germ line and the end row of continuous MES-4::GFP accumulating cells (at least 20 gonads were measured for each condition). ****$P < 1 \times 10^{-4}$ and *$P < 0.1$.

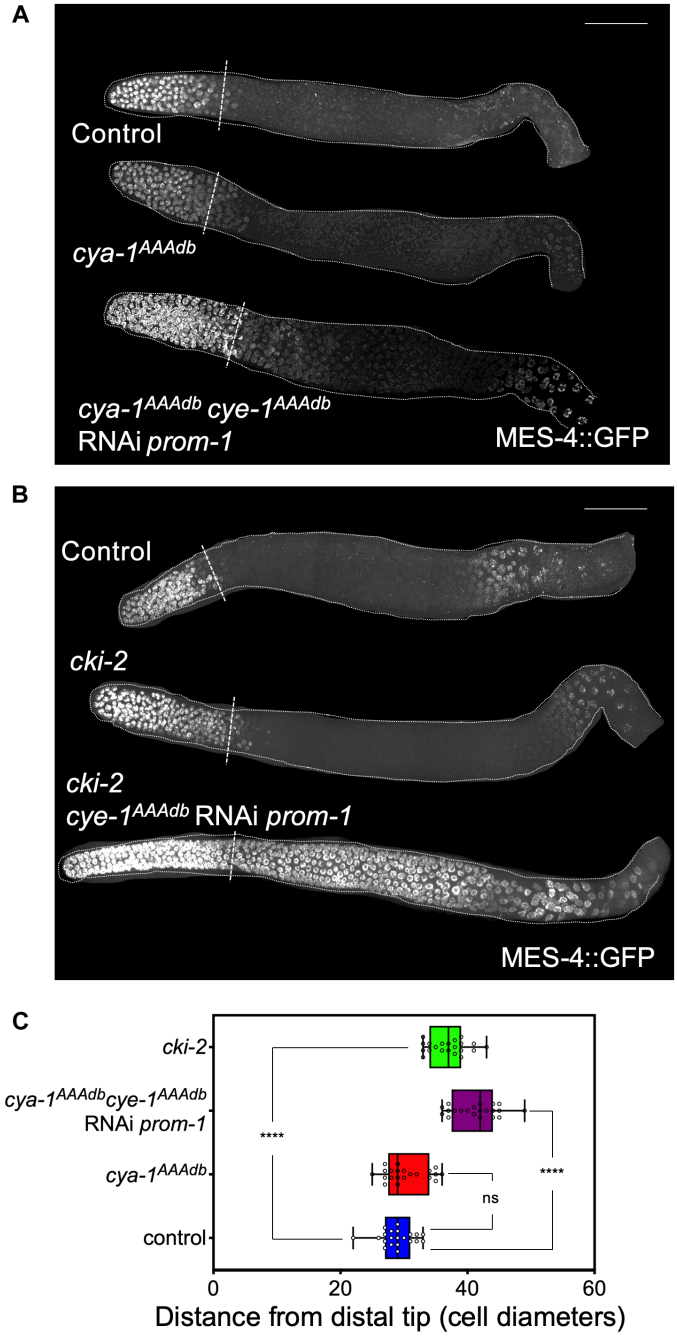

Fig. 8. The CDK inhibitor CKI-2 activates APC/C^{FZR-1} in cells reaching meiosis. (**A**) Stabilization of CYE-1 and CYA-1 levels does not impede the degradation of MES-4. Images of gonads dissected from young adult (1-day) worms carrying the *mes-4::gfp* allele in the indicated genetic backgrounds or RNAi conditions. Dashed lines indicate the PZ/TZ boundary defined by the morphology of DAPI-stained nuclei. Scale bar, 50 μm. (**B**) CKI-2 is required for the activation of APC/C^{FZR-1} when CYE-1 levels remain high. Images of gonads dissected from young adult (1-day) worms carrying the *mes-4::gfp* allele in the indicated genetic backgrounds or RNAi conditions. Dashed lines indicate the PZ/TZ boundary defined by the morphology of DAPI-stained nuclei. Scale bar, 50 μm. (**C**) Quantification of the distance (in germline cell diameters) between the distal tip of the germline and the end row of continuous MES-4::GFP-accumulating cells in the indicated genetic backgrounds (21 gonads were measured in each condition). ****$P < 1 \times 10^{-4}$.

kinase inhibitors from the CIP/KIP family: CKI-1 and CKI-2 (*46*). Of these, *cki-2* is expressed in the germ line; however, FBF proteins negatively regulate its mRNA in the PZ, resulting in its accumulation only in cells entering meiosis (*12*). The analysis of the *cki-2* mutant germlines showed that the MES-4::GFP fluorescent signal appeared more proximal compared to the control gonads (Fig. 8, B and C), although it drops in the medial part of the gonad. In contrast, when combined with *cye1*$^{AAA\ db}$ and RNAi of *prom-1*, the MES-4 signal was distributed along the entire length of the gonad (Fig. 8B). This suggests that APC/C^{FZR-1} was not activated in these conditions.

Together, these results show that APC/C^{FZR-1} is derepressed when cells enter meiosis, owing to the redundant effect of several independent mechanisms: (i) the increase in FZR-1 levels, (ii) the inhibition of CDK2 activity due to high levels of the CDK inhibitor CKI-2, (iii) the coordinated action on CYE-1 levels by the ubiquitin ligases SCF^{PROM-1} and APC/C^{FZR-1}.

MES-4 and MES-3 expression in the pachytene region may interfere with oogenesis

APC/C^{FZR-1} is primarily recognized as a cell cycle regulator that facilitates removal of various targets at the end of mitosis and in the early G_1 phase. Because many of these targets are crucial regulatory proteins that play significant roles during mitosis but become unnecessary in subsequent phases, the elimination of these proteins by APC/C^{FZR-1} prevents interference with cell cycle progression (*47*). We therefore entertained the idea that the role of APC/C^{FZR-1} in the germ line may involve removal of regulatory proteins, such as MES-4 and MES-3, that could obstruct activation of the oogenesis program once germ cells enter meiosis.

In agreement with published reports (*32*), we found that worms carrying the *fzr-1*(*ku298*) allele had a 50% smaller brood size than control worms (Fig. 9A). A transgenic line carrying an ectopic copy of *fzr-1* under the control of the *rps-27* promoter (which is expressed in the soma but not in the germline; fig. S14A) was not able to rescue this decrease in brood size (fig. S14B). Therefore, we attributed the brood size reduction to defects associated with the specific roles of APC/C^{FZR-1} in the germ line and not in the somatic gonad. Worms carrying *mes-3*^{AAA}, *mes-4*^{AAA}, or both showed only a modest decrease of 5 to 21% in brood size (Fig. 9A). We theorized that the differences in fertility between *fzr-1*(*ku298*) worms and those carrying the *mes-3*^{AAA} and *mes-4*^{AAA} alleles may reflect the involvement of additional unknown APC/C^{FZR-1} targets in the regulation of progeny production by the germ line.

A recent model proposed that MES-4 and PRC2 may protect germ line survival and proliferation by repressing an X-linked oogenesis program that may otherwise interfere with the development of nascent germ cells (*20*). In this model, the transcription factor LIN-15B may play an unknown role in launching the X-linked oogenesis program. We hypothesized that this program is counteracted by MES-4 and PRC2 in the distal gonad and released when the levels of these factors decrease in cells entering meiosis. This suggests that in *fzr-1*(*ku298*) mutants, the elevated levels of MES-4 and MES-3 (PRC2) in pachytene germ cells could interfere with activation of the oogenesis program. Consistent with this hypothesis, we found a strong synthetic effect on fertility in *fzr-1*(*ku298*) and *lin-15B*(*n744*) double mutants, which could be partially recapitulated in worms carrying the *mes-3*^{AAA} and *mes-4*^{AAA} alleles (Fig. 9A). To extend these observations, we used reverse transcription polymerase chain reaction (RT-PCR) to analyze the expression levels of

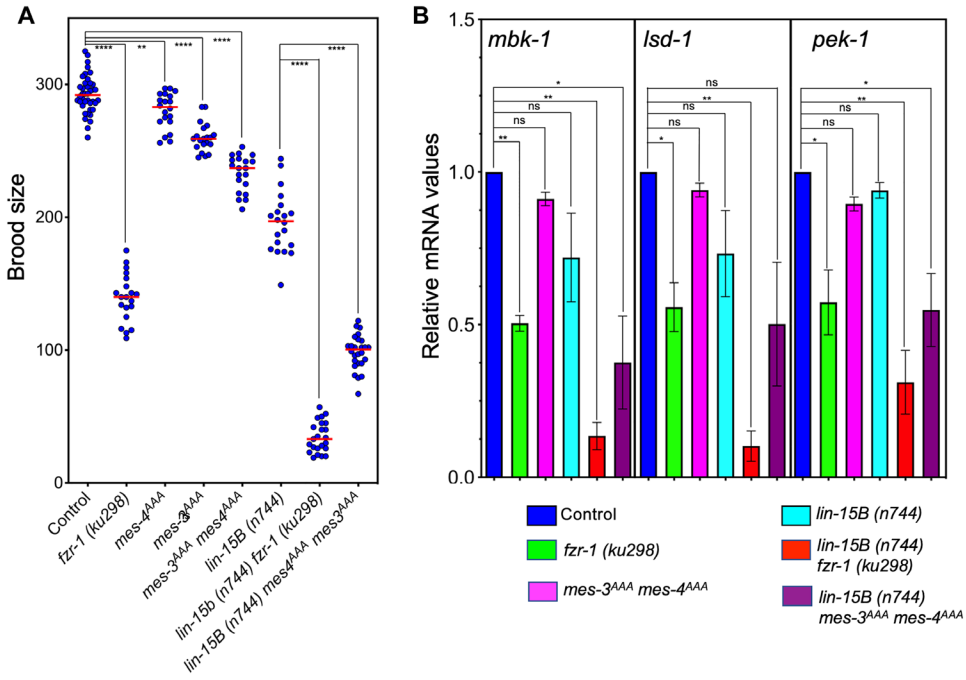

Fig. 9. MES-4 and MES-3 at the medial part of the gonad might interfere with the oogenesis program. (**A**) Stabilization of MES-4 and MES-3 at the pachytene has minimal impact on fertility but interacts genetically with *lin-15B*. The graph shows the brood size of wild-type, *fzr-1*(*ku298*), stabilized *mes-3*^{AAA} and *mes-4*^{AAA} alleles and combinations with the hypomorphic *lin-15B* (*n744*) allele. The graph shows the brood size of wild type (control) and the indicated allele combinations. Al least 20 worms were scored for each combination. (**B**) qRT-PCR of representative X-linked genes controlled by LIN-15B and MES-4/PCR2 in different mutant combinations. Values are based on the expression of each gene in gonads dissected from 1-day-old hermaphrodite adults N2 (control strain). Each column represents the mean value of three independent biological replicates. Error bars represent the SD. *$P < 0.1$, **$P < 1 \times 10^{-2}$, and ****$P < 1 \times 10^{-4}$.

three X-linked genes (*mbk-1*, *lsd-1*, and *pek-1*) that were proposed to be controlled by LIN-15B and MES-4/PRC2 (*22*). We found a clear correlation between the decreased mRNA levels of these genes and decreased brood size in their respective mutants (Fig. 9B).

DISCUSSION

The initial objective of this study was to understand the mechanism behind the decrease of MES-4 levels when germ cells enter meiosis in the gonads of *C. elegans*. An unexpected finding was that this protein decay was mediated by the E3 ubiquitin ligase complex APC/C, in interaction with its coactivator FZR-1. In addition, we found that APC/C^{FZR-1} similarly targets MES-3, a PRC2 component that also decreases upon onset of meiosis. These findings prompt questions about why APC/C^{FZR-1}, which is a cell-cycle regulator, is recruited to decrease the levels of these chromatin modifiers and how this E3 ubiquitin ligase complex is controlled to ensure the timely degradation of MES-4 and MES-3. Our study aimed to address these questions.

The APC/C E3 ubiquitin ligase primarily regulates the cell cycle, where it works sequentially, depending on the coactivator to which it binds. When associated with the Cdc20 coactivator at the onset of anaphase, APC/C first triggers sister chromatid separation by promoting degradation of Securin and Cyclin B, two inhibitors of Separase activity (*48*). Without Cdc20, cells arrest in metaphase (*49*). Later, when associated with the Cdh1/Fzr1 coactivator, APC/C promotes removal of many targets as cells exit mitosis and enter early G_1. These targets fall into two main classes: proteins with essential roles during mitosis with no role in the upcoming cell cycle phase (such as Cdc20, Geminin, or the kinases Aurora and Polo) and proteins whose levels must be limited to avoid premature accumulation during G_1 (such as Cyclins A and B) (*47*). Thus, APC/C$^{Cdh1/Fzr1}$ acts as a dedicated cleaning machinery that limits the presence of proteins that could otherwise interfere with the cell cycle. Although cells lacking Cdh1/Fzr1 can proliferate, they show defects in the cell cycle and genome stability. This likely occurs because of unwanted interactions caused by the persistence of certain cell cycle regulators (*50*, *51*).

In line with the regulatory role of APC/C$^{Cdh1/Fzr1}$ in the cell cycle, we have found that CYE-1 and CYA-1, the cyclins for S phase and S/G_2 phase, respectively, are targets of APC/C^{FZR-1} in the *C. elegans* germ line, once cells enter the meiotic cell cycle. Decreasing S-phase cyclins during meiotic prophase I may prevent unwanted interference with subsequent meiotic stages.

We found that APC/C targets FZR-1 degradation, and its inability to do so markedly reduced fertility. Although APC/C targeting of Cdh1/Fzr1 has been described in other systems (*35*, *52*), we can only speculate about why FZR-1 must be degraded as germ cells transition to meiosis in *C. elegans*. Our study showed that the primary obstacle to APC/C^{FZR-1} activity in mitotically dividing germ cells is CDK2 activity. However, CDK2 activity markedly decreases when cells enter meiosis because of decreased CYE-1 and CYA-1 levels and increased CKI-2 activity. In this context, where APC/C^{FZR-1} itself is not significantly inhibited, FZR-1 degradation makes sense to prevent unscheduled targeting of proteins essential for meiosis. One potential target could be Geminin (GMN-1), a well-described target

of APC/$C^{Cdh1/Fzr1}$ in other systems; consistent with this same regulation in worms, the GMN-1 sequence harbors a destruction box. In addition, RNAi silencing results in an aberrant germline with a severe oogenesis defect (*53*).

A major discovery reported in this work is that APC/C^{FZR-1} targets degradation of MES-4 and MES-3, two well-defined chromatin regulators in *C. elegans* mitotically dividing germ cells. Although unexpected, this result is not illogical. It was unexpected because few chromatin modifiers have been identified so far as targets of APC/C complexed with Cdh1/Fzr1. One is mammalian Ki-67, a protein involved in structuring heterochromatin that is cleared from constitutive heterochromatin as cells exit mitosis during neuronal differentiation. APC/C^{Cdh1} performs this clearance, and defects in that degradation alter heterochromatin, nuclear architecture, and gene expression, resulting in severe defects in brain development (*54*, *55*). A second is *Saccharomyces cerevisiae* Set1, an H3K4 histone methyltransferase that promotes the transcription of histone genes, which is a target of APC/C^{CDH1}. Set1 degradation prevents premature synthesis and accumulation of potentially cytotoxic core histones during G_1 (*56*). These targets align with the proposed role of APC/C complexed with Cdh1/Fzr1, working as a specific system to decrease the levels of certain proteins, control their activity, and prevent unwanted interference. Similarly in *C. elegans*, APC/C^{FZR-1} directed degradation of MES-4 and MES-3 may limit these chromatin regulatory proteins, whose roles in mitotic germ cells could interfere with meiotic germ cells and oogenesis. The recently proposed functions of MES-4 and PRC2 as negative regulators of an X-linked oogenesis program (*20*) highlight the need for their degradation. Consistent with our findings, APC/C^{FZR-1} activity may facilitate the transition from undifferentiated germ cells to oocytes by lifting repression in cells entering meiosis. In addition, decrease of the levels of MES-4, MES-3, and other targets that remain unknown by APC/C^{FZR-1} could facilitate the reprogramming of germ cells into oocytes. The dynamic remodeling of histone modifications as germ cells differentiate into oocytes has been described (*57*), suggesting a mechanism for establishing an early transcriptional program to trigger zygotic genome activation. Transiently decreasing the levels of chromatin modifiers such as MES-4 and PCR2 from early to late pachytene provides an opportunity for the establishment of an alternative epigenetic landscape in oocytes.

An intriguing question stemming from our findings is why the APC/C^{FZR-1} E3 ubiquitin ligase is used to eliminate MES-4 and MES-3. Why not other E3 ubiquitin ligases that are also active in the germline, such as RFP-1 or the SCF^{PROM-1} complex? A crucial point to consider when exploring this question is that APC/C^{FZR-1} may also serve to communicate cell cycle status. Despite its role as a cell cycle regulator, APC/$C^{Cdh1/Fzr1}$ does not initiate any cell cycle transition (unlike APC/C^{Cdc20}). Conversely, because CDK phosphorylation negatively affects the Cdh1/Fzr1 interaction with the APC/C core, APC/$C^{Cdh1/Fzr1}$ activity is restricted from the end of mitosis (when CDK activity begins to decrease) to late G_1 phase (when CDK activity starts to rise). In other words, APC/$C^{Cdh1/Fzr1}$ activity is linked to cell cycle exit. By placing MES-4 and MES-3 under regulation of APC/C^{FZR-1}, these chromatin regulators remain active during the mitotic cell cycle, which is maintained by the CDK2 complex. However, once germ cells initiate the meiotic program, a reduction in CDK2 activity triggers activation of APC/C^{FZR-1}. This, in turn, leads to the decrease of MES-4 and MES-3 levels.

An important element in this regulation is the negative feedback loop between CDK-2/CYE-1 and APC/C^{FZR-1}, which is unique to *C. elegans*. Although Cdk2/Cyclin E inhibition of APC/$C^{Cdh1/Fzr1}$ is widely conserved [reviewed in (*58*)], cyclin E was not identified as a substrate of APC/$C^{Cdh1/Fzr1}$ in *S. cerevisiae* (Clb5 and Clb6) (*59*), *Drosophila* (*43*), or vertebrates (*60*). Mutual repression is a classical network motif in developmental processes and serves as a "toggle switch" for regulating changes between the two states (*61*). However, the mutual repression between APC/C^{FZR-1} and CDK-2/CYE-1 in *C. elegans* changes with position within the germ line and therefore does not provide a simple toggle switch. Rather, we propose that this mutual repression acts more as a teeter-totter that shifts the balance between on/off degradation of chromatin regulators (among other targets) depending on the germline region (Fig. 10A).

Low FZR-1 levels in mitotically dividing germ cells rely on Notch signaling, its activation of LST-1 and SYGL-1 and their partnerships with FBF proteins. FBF/LST-1 and FBF/SYGL-1 are well-established RNA repressors and likely repress *fzr-1* expression via interactions with the *fzr-1* 3′UTR (*36*). In addition, FBF inhibits *cki-2* mRNA translation (*12*) and helps maintain high CYE-1 by promoting translation, indirectly through inhibition of GLD-1 (*11*). The CDK2-APC/C^{FZR-1} balance in mitotic germ cells favors accumulation of phosphorylated FZR-1 and thus inactive APC/C^{FZR-1} in this region. As germ cells move away from the influence of the niche and approach the TZ, an increase in activity of the *fzr-1* promoter coincides with a decrease in FBF-mediated repression, resulting in higher FZR-1 as germ cells enter the meiotic cell cycle. In addition to the CDK-2/CYE-2 activity decrease and FZR-1 increase in this region, the appearance of SCF^{PROM-1} is supplemented with the rise in CKI-2 and likely in GLD-1. Under these conditions, nonphosphorylated forms of FZR-1 accumulate. Upon binding to the APC/C core, CYE-1 degradation is enhanced, shifting the balance between CDK and APC/C^{FZR-1} in favor of full activity of the E3 ubiquitin ligase. This shift, which occurs as germ cells enter meiosis, promotes degradation of MES-4 and MES-3.

The negative feedback loop between CDK-2/CYE-1 and APC/C^{FZR-1} reported here resembles the negative feedback loop between GLD-1 and CDK-2/CYE-1 (*62*). Furthermore, CDK phosphorylation negatively regulates Cyclin-dependent kinase inhibitors (CKIs) in *C. elegans* (*63*), suggesting existence of a similar negative feedback loop for CKI-2 as well. The balance of each negative feedback loop shifts as cells leave influence of the niche. A reduction in the inhibitory effect of FBF on the levels of GLD-1, CKI-2, and FZR-1, in conjunction with activity of SCF^{PROM-1}, drives this shift. PROM-1 levels increase as cells approach the TZ (*64*), and likely, it acts as a trigger to initiate the decrease in CDK activity. All these negative loops operate in a coordinated manner but appear to be independent of each other, making the timing of the down-regulation of CDK-2/CYE-1 activity and, thereby, the release of APC/C^{FZR-1} very robust (Fig. 10B). This observation aligns with the idea that redundancy is a common feature in the decision-making process between proliferation and meiosis in *C. elegans* (*65*).

Cdh1/Fzr1 is essential for the development of multicellular organisms, and its absence has been linked to defective cell differentiation [reviewed in (*24*, *47*)]. However, it remains unclear whether these differentiation defects result from abnormalities in the cell cycle or lack of degradation of targets in the differentiation process, such as Myf5 in muscles (*66*), Id2 in neurogenesis (*67*), or SnoN in

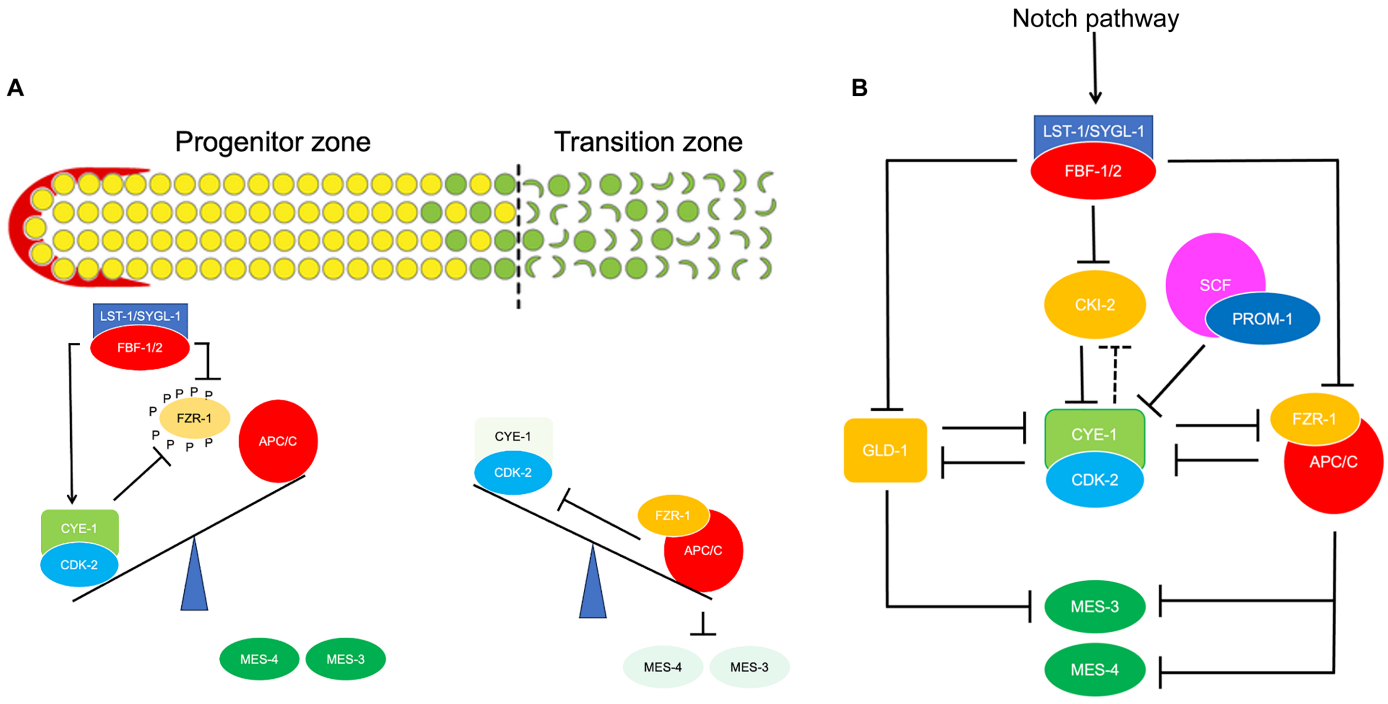

Fig. 10. The working model of APC/C^{FZR-1} regulation in the distal gonad of *C. elegans*. (**A**) A cartoon showing how the negative feedback loop between CDK-2/CYE-1 and APC/C^{FZR-1} acts as a cellular teeter-totter, shifting the balance between on/off degradation of chromatin regulators (among other targets) depending on which gonad region the cell is located. (**B**) Scheme showing how different pathways, all under Notch control, act coordinately to enable the activation of APC/C^{FZR-1}. Dashed lines indicate predicted genetic interactions.

the lens (*68*). Our study, which identifies MES-4 and MES-3 as targets of APC/C^{FZR-1}, suggests that the lack of degradation of targets that repress differentiation causes these defects. However, the two explanations are not mutually exclusive.

The APC/C$^{Cdh1/Fzr1}$ complex is present but inactive in undifferentiated cells, particularly in stem cells, but its activity significantly increases during differentiation (reviewed in (*69*)). This increase was thought to result from G1 phase elongation, which typifies differentiation (*70*). The G1 phase is when Cdh1/Fzr1 interacts with the APC/C core. However, our findings challenge this perspective. One of the key conclusions of our study is that the DTC, which provides the niche in this system, regulates APC/C^{FZR-1} activity through Notch signaling and its downstream effectors. By analogy, an attractive hypothesis is that stem cell niches maintain properties of stemness by suppressing activity of the Cdh1/Fzr1-associated APC/C complex. When stem cells leave their niche, this Cdh1/Fzr1 suppression is lifted, thus facilitating differentiation. Investigating niche-mediated down-regulation of Cdh1/Fzr1 could thus enhance our understanding of how stem cell niches promote stemness and warrants further exploration in other experimental systems.

Limitations of the study

This study had some limitations. The first was the incomplete characterization of the biological consequences of absence of APC/C^{FZR-1} activity in gonads. Given the significant role of Cdh1/Fzr1 in differentiation in other organisms, we observed that worms carrying the *fzr-1*(*ku298*) allele had a modest reduction in fertility, producing only about half as many offspring as wild-type worms. We attributed this to the hypomorphic nature of this allele. The molecular defect in this mutant allele is a single amino acid change in one of the β-propellers of WD40 repeats (C526Y) (*32*). WD40 repeats are involved in the recognition of substrates (*38*). Although the mutation in *ku298* most likely affects recognition of substrates such as MES-4 and MES-3, it is possible that other important substrates remain unaffected by this mutation. We have created a complete loss-of-function allele of *fzr-1* by deleting the entire open reading frame. However, this mutant causes a severe defect in determining the fate of the DTC and hence has essentially no germline tissue. Therefore, future studies of this mutant must differentiate defects in the somatic gonad from defects in the germline to fully elucidate the germline role of FZR-1.

The combination of the *mes-4*^{AAA} and *mes-3*^{AAA} alleles did not replicate the fertility defects observed in *ku298* worms, suggesting the possibility of additional unknown targets. Besides the ability to methylate histones via catalytic complexes, essential factors for interpreting histone modifications are the effectors or readers that connect the chromatin landscape to functional outcomes (*71*). We hypothesized that APC/C^{FZR-1} removes histone methylation readers in addition to the catalytic subunits when the cells enter meiosis. Thus, the observed low impact of high levels of MES-4 and MES-3 in the pachytene region could be attributed to the degradation of histone modification readers by APC/C^{FZR-1}. We believe that more significant effects may be observed if both the catalytic subunits and the histone-modification readers were stabilized simultaneously. A recent systematic characterization of chromodomain proteins in *C. elegans* identified several putative readers of diverse histone methylation marks (*72*). Some of these chromodomain-containing proteins (UAD-2, SET-31, CEC-7, and CEC-9) are expressed in the germ line, recognize marks made by MES-4 or PCR2 and contain

putative KEN or destruction boxes in their sequences. However, further study is needed to determine whether the APC/C^{FZR-1} targets these proteins.

MATERIALS AND METHODS

Nematode strain, strain constructions, and culture conditions

All strains used in this work were derivatives of N2 Bristol (table S1). Standard culture conditions were used, with maintenance at 20°C unless otherwise stated (*73*). CRISPR editing and MOS integration were performed as described previously (*74*, *75*). The construction of transgenes and generation of transgenic lines are described in the Supplementary Materials. The guide and repair templates, along with other primers used in this study, are listed in table S2.

Cytological preparation of gonads for direct observation and immunostaining

All procedures are based on previously published protocols described in (*76*). Worms were dissected as young adults (24 hours after the L4 stage of development) unless otherwise stated. The worms were synchronized using a bleaching protocol to reduce experimental variability. Synchronized young adults were selected and placed in a tube of phosphate-buffered saline (PBS) and 0.1% Tween 20 (PBST) supplemented with 0.1% levamisole to allow partial immobilization of the worms. After 5 min, the worms were transferred to a petri dish filled with PBST and dissected by cutting the head at the pharyngeal level with a scalpel and consequently expelling the gonad from the interior of the worms. Gonads were collected and transferred to new tubes for further experiments.

The collected gonads were partially fixed in methanol at −20°C for 5 min for direct observation of fluorescent proteins. They were centrifuged in a benchtop centrifuge and washed thrice with PBST. Next, they were stained in 4′,6-diamidino-2-phenylindole (DAPI) (0.5 μg/ml) diluted in PBST for 5 min; they were then centrifuged, and most liquid removed from the tube to enable transfer of gonads to a 2% agarose pad on a slide. A mounting agent (VECTASHIELD) was added to each corner of the agarose pad, and a cover slip was gently placed on top of the sample, which was then sealed with nail polish spread on the coverslip edges.

Immunostaining of V5::FZR-1 worms (Fig. 4, A and B) was performed as previously described (*76*). Briefly, gonads were fixed in 2% paraformaldehyde for 10 min. They were then centrifuged at 4400 rpm for 1 min and placed in methanol at −20°C. After 5 min, the samples were centrifuged, and methanol was removed. The gonads were then incubated with a blocking solution [PBST and 0.5% bovine serum albumin (BSA)] for 1 hour. Next, they were incubated overnight at 4°C with the primary antibody mix diluted in blocking solution. Specific primary antibodies were used at the concentrations recommended by the manufacturer. Mouse anti-V5 (MCA1360, Bio-Rad) was used at 1:1000 to 1:5000; rabbit anti-GFP (ab290, Abcam) was used at 1:200. The following day, gonads were centrifuged, the primary antibody mix removed, and samples washed three times with PBST for 3 to 5 min. Gonads were subsequently incubated in the dark for 1 hour with a secondary antibody mix composed of PBST, 0.5% BSA, DAPI, and secondary antibodies αMouse-Alexa647 (1:1000; A-31571, Molecular Probes/Invitrogen) and anti–Rabbit-Alexa Fluor 488 (1:1000; A-21206, Molecular Probes/Invitrogen). Gonads were centrifuged, the secondary antibody mix removed, and samples washed four times with PBST for 3 to 5 min. After the final wash, gonads were left in only 10 μl of PBST. A drop of ProLong Gold antifade mounting medium was added and gently mixed. Gonads were then placed on a slide, bubbles and excess liquid were removed, and a cover was gently placed on top. The samples were left to cure for at least 1 day.

Immunostaining of MES-4 (figs. S1 and S4) was performed as previously described (*77*). Dissected gonads were fixed through freeze cracking on poly-L-lysine–coated slides, followed by methanol and acetone incubation at 4°C (10 min each). The slides were allowed to dry and then blocked with 1.5% ovalbumin and 1.5% BSA in PBS at room temperature for 30 min. Samples were incubated with the primary antibody (Rabbit–anti–MES-4; 1:400) overnight at 4°C in PBST. The next day, the slides were washed thrice with PBST, blocked again for 10 min, and incubated in the dark with a secondary antibody (αRabbit-Alexa488, 1:1000; A-21206, Molecular Probes/Invitrogen) and DAPI for 2 hours. The slides were washed and mounted in a polyvinyl alcohol solution for imaging 1 day later.

Microscopy

All procedures are described in (*76*). Gonads were imaged using an Olympus IX81 confocal spinning disk (Yokogawa CSU-X1 disk unit equipped with a photometrics evolve electron multiplying charge-coupled device camera) with the Metamorph software. Immunostained gonads were imaged using a Leica SP8 confocal scanning laser with LAS X software.

Z-stack images were converted into Z-max projections using the FIJI software. Olympus spinning disk images require stitching to observe the full gonad in a single image. The images were stitched together using Stitching plugin in FIJI. In some cases (fig. S13B), when the intensity of the signal was very low, the stitching of images to build up the entire gonad was performed manually using Adobe Photoshop. In these cases, the fluorescence levels of the stitched images were adjusted in Adobe Photoshop to correct for the auto-adjustment settings of the microscope. The Leica SP8 images required no stitching because the field of vision and zoom were appropriate for capturing the full gonads in a single image. PZ size was scored in DAPI-stained dissected gonads. Briefly, the PZ/TZ boundary was defined as the distal-most row of cells containing multiple nuclei with crescent-shaped DAPI morphology. The quantification of protein levels is described in the Supplementary Methods.

RNA interference

Procedures are described in (*76*). RNAi was used to silence gene expression. RNAi was introduced into worms by feeding them the *Escherichia coli* strain HT115 with different RNAi-producing plasmids. These strains were either obtained from Ahringer's library or constructed by cloning 0.5- to 1-kb gene fragments into pL4440 and then transforming the constructed plasmid into HT115. To silence multiple genes, up to three gene fragments of 0.5 to 1 kb were cloned in tandem into a multicloning site in pL4440. HT115 cells with different pL4440 plasmids were grown overnight at 37°C in LB medium supplemented with ampicillin (200 mg/liter). The culture was concentrated 10 times and placed on nematode growth medium (NGM) plates containing isopropyl-β-D-thiogalactopyranoside (50 mg/liter) and ampicillin (200 mg/liter). RNAi plates were incubated at room temperature for 1 day before the worms were added.

Synchronized L4s were placed on NGM plates seeded with double-stranded RNA–expressing or empty vector control bacteria and incubated at 20°C. We dissected gonads after 24 hours.

RNA extraction and qRT-PCR

RNA was extracted from ~50 gonads dissected from 1-day-old hermaphrodite adults as previously described (*20*). Isolated gonads were incubated in 500 µl of TRIzol reagent, flash-frozen in liquid nitrogen, and stored at −80°C before RNA extraction. To release RNAs from gonads in TRIzol, gonads were freeze-thawed three times using liquid nitrogen and a 37°C water bath while vortexing vigorously between cycles. This solution was mixed with phase-lock heavy gel and 100 µl of 1-bromo-3-chloropropane and incubated at room temperature for 10 min. Samples were then centrifuged at 13,000 rpm and 4°C for 15 min to separate phases. RNAs in the aqueous phase were precipitated by mixing well with 0.8 volumes of ice-cold isopropanol and 1 µl of glycogen (20 mg/ml), followed by incubation at −80°C for 1 to 2 hours and centrifugation at 13,000 rpm for 30 min at 4°C. RNA pellets were washed thrice with ice-cold 75% ethanol and then resuspended in 15 µl of water.

cDNA was synthesized using the high-capacity cDNA Reverse Transcription Kit (Applied Biosystems, Waltham, MA, USA) with 1 mg of total RNA per sample. qRT-PCR was performed using the Sso Advanced Universal SYBR Green Supermix (Bio-Rad) in a CFX96 Real-Time PCR System (Bio-Rad). Reaction conditions were as follows: 3 min at 95°C, followed by 40 cycles of 10 s at 95°C, 10 s at 60°C, and 30 s at 72°C. The relative levels of the analyzed mRNAs in the mutant strains were calculated using the ΔΔCt method with *tbb-2* expression and normalized to the wild-type control. The list of primers used for qRT-PCR is shown in table S2.

Determination of brood size

Individual L4 hermaphrodites were transferred to separate plates for brood size assessment. They were moved to new plates every 48 hours for 8 days, and progeny was counted in each plate. Unhatched embryos were allowed another 24 hours to hatch and develop, after which unhatched embryos were counted as dead and hatched progeny as living. The total brood size of each mother was calculated as the sum of both living and dead progeny.

Prediction of KEN-box and D-box motifs

We used GPS-ARM 1.0 to validate the presence of KEN- or D-box motifs in the protein. This software predicts the existence of both KEN-boxes and D-boxes and assigns them a score based on previously identified boxes (*78*).

Quantification and statistical analysis

We used GraphPad PRISM 6 for statistical analysis. GraphPad PRISM 6 software was also used to determine brood size and expression graphs. Graphs show all individual values, the median and the standard deviation. Two-tailed unpaired Student's *t* tests were performed when data passed the Shapiro and Kolmogorov-Smirnov normality tests and when sample variance was equal; two-tailed Welch's *t* tests were performed when data passed the Shapiro and Kolmogorov-Smirnov normality tests and when sample variance was unequal; two-tailed nonparametric Mann-Whitney tests were performed when data did not pass the Shapiro or Kolmogorov-Smirnov normality test.

Supplementary Materials

This PDF file includes:

Supplementary Methods
Figs. S1 to S14
Tables S1 and S2
References

REFERENCES AND NOTES

1. C. A. Chacón-Martínez, J. Koester, S. A. Wickström, Signaling in the stem cell niche: Regulating cell fate, function and plasticity. *Development* **145**, dev165399 (2018).
2. G. B. Adams, R. P. Martin, I. R. Alley, K. T. Chabner, K. S. Cohen, L. M. Calvi, H. M. Kronenberg, D. T. Scadden, Therapeutic targeting of a stem cell niche. *Nat. Biotechnol.* **25**, 238–243 (2007).
3. S. J. Morrison, A. C. Spradling, Stem cells and niches: Mechanisms that promote stem cell maintenance throughout life. *Cell* **132**, 598–611 (2008).
4. J. Kimble, C. Nüsslein-Volhard, The great small organisms of developmental genetics: *Caenorhabditis elegans* and *Drosophila melanogaster*. *Dev. Biol.* **485**, 93–122 (2022).
5. J. Kimble, H. Seidel, *C. elegans* germline stem cells and their niche, in *StemBook*, J. Kimble, H. Seidel, Eds. (Harvard Stem Cell Institute, 2008).
6. E. J. A. Hubbard, T. Schedl, Biology of the *Caenorhabditis elegans* germline stem cell system. *Genetics* **213**, 1145–1188 (2019).
7. A. S. Ferdous, T. R. Lynch, S. J. C. Costa Dos Santos, D. H. Kapadia, S. L. Crittenden, J. Kimble, LST-1 is a bifunctional regulator that feeds back on Notch-dependent transcription to regulate *C. elegans* germline stem cells. *Proc. Natl. Acad. Sci. U.S.A.* **120**, e2309964120 (2023).
8. A. S. Ferdous, S. J. Costa Dos Santos, C. R. Kanzler, H. Shin, B. H. Carrick, S. L. Crittenden, M. Wickens, J. Kimble, The in vivo functional significance of PUF hub partnerships in *C. elegans* germline stem cells. *Development* **150**, dev201705 (2023).
9. P. M. Fox, V. E. Vought, M. Hanazawa, M.-H. Lee, E. M. Maine, T. Schedl, Cyclin E and CDK-2 regulate proliferative cell fate and cell cycle progression in the *C. elegans* germline. *Development* **138**, 2223–2234 (2011).
10. T. Furuta, H. J. Joo, K. A. Trimmer, S. Y. Chen, S. Arur, GSK-3 promotes S-phase entry and progression in *C. elegans* germline stem cells to maintain tissue output. *Development* **145**, (2018).
11. B. Biedermann, J. Wright, M. Senften, I. Kalchhauser, G. Sarathy, M. H. Lee, R. Ciosk, Translational repression of cyclin E prevents precocious mitosis and embryonic gene activation during *C. elegans* meiosis. *Dev. Cell* **17**, 355–364 (2009).
12. I. Kalchhauser, B. M. Farley, S. Pauli, S. P. Ryder, R. Ciosk, FBF represses the Cip/Kip cell-cycle inhibitor CKI-2 to promote self-renewal of germline stem cells in *C. elegans*. *EMBO J.* **30**, 3823–3829 (2011).
13. Y. Fong, L. Bender, W. Wang, S. Strome, Regulation of the different chromatin states of autosomes and X chromosomes in the germ line of *C. elegans*. *Science* **296**, 2235–2238 (2002).
14. L. Xu, J. Paulsen, Y. Yoo, E. B. Goodwin, S. Strome, *Caenorhabditis elegans* MES-3 is a target of GLD-1 and functions epigenetically in germline development. *Genetics* **159**, 1007–1017 (2001).
15. L. B. Bender, R. Cao, Y. Zhang, S. Strome, The MES-2/MES-3/MES-6 complex and regulation of histone H3 methylation in *C. elegans*. *Curr. Biol.* **14**, 1639–1643 (2004).
16. L. Xu, Y. Fong, S. Strome, The *Caenorhabditis elegans* maternal-effect sterile proteins, MES-2, MES-3, and MES-6, are associated in a complex in embryos. *Proc. Natl. Acad. Sci. U.S.A.* **98**, 5061–5066 (2001).
17. L. B. Bender, J. Suh, C. R. Carroll, Y. Fong, I. M. Fingerman, S. D. Briggs, R. Cao, Y. Zhang, V. Reinke, S. Strome, MES-4: An autosome-associated histone methyltransferase that participates in silencing the X chromosomes in the *C. elegans* germ line. *Development* **133**, 3907–3917 (2006).
18. A. Rechtsteiner, S. Ercan, T. Takasaki, T. M. Phippen, T. A. Egelhofer, W. Wang, H. Kimura, J. D. Lieb, S. Strome, The histone H3K36 methyltransferase MES-4 acts epigenetically to transmit the memory of germline gene expression to progeny. *PLOS Genet.* **6**, e1001091 (2010).
19. S. Strome, D. Updike, Specifying and protecting germ cell fate. *Nat. Rev. Mol. Cell Biol.* **16**, 406–416 (2015).
20. C. S. Cockrum, S. Strome, Maternal H3K36 and H3K27 HMTs protect germline development via regulation of the transcription factor LIN-15B. *eLife* **11**, e77951 (2022).
21. C.-Y. S. Lee, T. Lu, G. Seydoux, Nanos promotes epigenetic reprograming of the germline by down-regulation of the THAP transcription factor LIN-15B. *eLife* **6**, e30201, e30201 (2017).
22. V. J. Robert, A. K. Knutson, A. Rechtsteiner, S. Garvis, G. Yvert, S. Strome, F. Palladino, *Caenorhabditis elegans* SET1/COMPASS maintains germline identity by preventing transcriptional deregulation across generations. *Front. Cell Dev. Biol.* **8**, 561791 (2020).
23. J. Pines, Cubism and the cell cycle: The many faces of the APC/C. *Nat. Rev. Mol. Cell Biol.* **12**, 427–438 (2011).
24. Y. Kimata, APC/C ubiquitin ligase: Coupling cellular differentiation to G1/G0 phase in multicellular systems. *Trends Cell Biol.* **29**, 591–603 (2019).
25. C. Merritt, D. Rasoloson, D. Ko, G. Seydoux, 3′ UTRs are the primary regulators of gene expression in the *C. elegans* germline. *Curr. Biol.* **18**, 1476–1482 (2008).
26. K. Theil, M. Herzog, N. Rajewsky, Post-transcriptional regulation by 3′ UTRs can be masked by regulatory elements in 5′ UTRs. *Cell Rep.* **22**, 3217–3226 (2018).
27. L. D. Macdonald, A. Knox, D. Hansen, Proteasomal regulation of the proliferation vs. meiotic entry decision in the *Caenorhabditis elegans* germ line. *Genetics* **180**, 905–920 (2008).

28. N. Papaevgeniou, N. Chondrogianni, The ubiquitin proteasome system in *Caenorhabditis elegans* and its regulation. *Redox Biol.* **2**, 333–347 (2014).
29. P. Gupta, L. Leahul, X. Wang, C. Wang, B. Bakos, K. Jasper, D. Hansen, Proteasome regulation of the chromodomain protein MRG-1 controls the balance between proliferative fate and differentiation in the *C. elegans* germ line. *Development* **142**, 291–302 (2015).
30. A. Mohammad, K. Vanden Broek, C. Wang, A. Daryabeigi, V. Jantsch, D. Hansen, T. Schedl, Initiation of meiotic development is controlled by three post-transcriptional pathways in *Caenorhabditis elegans*. *Genetics* **209**, 1197–1224 (2018).
31. A. Golden, P. L. Sadler, M. R. Wallenfang, J. M. Schumacher, D. R. Hamill, G. Bates, B. Bowerman, G. Seydoux, D. C. Shakes, Metaphase to anaphase (mat) transition-defective mutants in *Caenorhabditis elegans*. *J. Cell Biol.* **151**, 1469–1482 (2000).
32. D. S. Fay, S. Keenan, M. Han, *fzr-1* and *lin-35*/Rb function redundantly to control cell proliferation in *C. elegans* as revealed by a nonbiased synthetic screen. *Genes Dev.* **16**, 503–517 (2002).
33. R. Kitagawa, E. Law, L. Tang, A. M. Rose, The Cdc20 homolog, FZY-1, and its interacting protein, IFY-1, are required for proper chromosome segregation in *Caenorhabditis elegans*. *Curr. Biol.* **12**, 2118–2123 (2002).
34. J. E. Wright, D. Gaidatzis, M. Senften, B. M. Farley, E. Westhof, S. P. Ryder, R. Ciosk, A quantitative RNA code for mRNA target selection by the germline fate determinant GLD-1. *EMBO J.* **30**, 533–545 (2011).
35. D. Ostapenko, M. J. Solomon, APC^{Cdh1}-mediated degradation of Cdh1 is necessary for faithful meiotic chromosome segregation in *S. cerevisiae*. bioRxiv 601619 [Preprint] (2024); https://doi.org/10.1101/2024.07.01.601619.
36. A. Prasad, D. F. Porter, P. L. Kroll-Conner, I. Mohanty, A. R. Ryan, S. L. Crittenden, M. Wickens, J. Kimble, The PUF binding landscape in metazoan germ cells. *RNA* **22**, 1026–1043 (2016).
37. L. Chang, Z. Zhang, J. Yang, S. H. McLaughlin, D. Barford, Atomic structure of the APC/C and its mechanism of protein ubiquitination. *Nature* **522**, 450–454 (2015).
38. C. Alfieri, S. Zhang, D. Barford, Visualizing the complex functions and mechanisms of the anaphase promoting complex/cyclosome (APC/C). *Open Biol.* **7**, (2017).
39. I. The, S. Ruijtenberg, B. P. Bouchet, A. Cristobal, M. B. W. Prinsen, T. van Mourik, J. Koreth, H. Xu, A. J. R. Heck, A. Akhmanova, E. Cuppen, M. Boxem, J. Muñoz, S. van den Heuvel, Rb and FZR1/Cdh1 determine CDK4/6-cyclin D requirement in *C. elegans* and human cancer cells. *Nat. Commun.* **6**, 5906 (2015).
40. E. T. Kipreos, S. van den Heuvel, Developmental control of the cell cycle: Insights from *Caenorhabditis elegans*. *Genetics* **211**, 797–829 (2019).
41. S. Höckner, L. Neumann-Arnold, W. Seufert, Dual control by Cdk1 phosphorylation of the budding yeast APC/C ubiquitin ligase activator Cdh1. *Mol. Biol. Cell* **27**, 2198–2212 (2016).
42. J. D. Reimann, B. E. Gardner, F. Margottin-Goguet, P. K. Jackson, Emi1 regulates the anaphase-promoting complex by a different mechanism than Mad2 proteins. *Genes Dev.* **15**, 3278–3285 (2001).
43. R. Grosskortenhaus, F. Sprenger, Rca1 inhibits APC-Cdh1(Fzr) and is required to prevent cyclin degradation in G2. *Dev. Cell* **2**, 29–40 (2002).
44. A. Reber, C. F. Lehner, H. W. Jacobs, Terminal mitoses require negative regulation of Fzr/Cdh1 by cyclin A, preventing premature degradation of mitotic cyclins and String/Cdc25. *Development* **133**, 3201–3211 (2006).
45. P. M. Fox, T. Schedl, Analysis of germline stem cell differentiation following loss of GLP-1 Notch activity in *Caenorhabditis elegans*. *Genetics* **201**, 167–184 (2015).
46. Y. Hong, R. Roy, V. Ambros, Developmental regulation of a cyclin-dependent kinase inhibitor controls postembryonic cell cycle progression in *Caenorhabditis elegans*. *Development* **125**, 3585–3597 (1998).
47. X. Qiao, L. Zhang, A. M. Gamper, T. Fujita, Y. Wan, APC/C-Cdh1: From cell cycle to cellular differentiation and genomic integrity. *Cell Cycle* **9**, 3904–3912 (2010).
48. K. Nasmyth, Segregating sister genomes: The molecular biology of chromosome separation. *Science* **297**, 559–565 (2002).
49. M. Li, J. P. York, P. Zhang, Loss of Cdc20 causes a securin-dependent metaphase arrest in two-cell mouse embryos. *Mol. Cell. Biol.* **27**, 3481–3488 (2007).
50. I. García-Higuera, E. Manchado, P. Dubus, M. Cañamero, J. Méndez, S. Moreno, M. Malumbres, Genomic stability and tumour suppression by the APC/C cofactor Cdh1. *Nat. Cell Biol.* **10**, 802–811 (2008).
51. R. Sigl, C. Wandke, V. Rauch, J. Kirk, T. Hunt, S. Geley, Loss of the mammalian APC/C activator FZR1 shortens G1 and lengthens S phase but has little effect on exit from mitosis. *J. Cell Sci.* **122**, 4208–4217 (2009).
52. T. Listovsky, Y. S. Oren, Y. Yudkovsky, H. M. Mahbubani, A. M. Weiss, M. Lebendiker, M. Brandeis, Mammalian Cdh1/Fzr mediates its own degradation. *EMBO J.* **23**, 1619–1626 (2004).
53. K. Yanagi, T. Mizuno, T. Tsuyama, S. Tada, Y. Iida, A. Sugimoto, T. Eki, T. Enomoto, F. Hanaoka, *Caenorhabditis elegans* geminin homologue participates in cell cycle regulation and germ line development. *J. Biol. Chem.* **280**, 19689–19694 (2005).
54. C. J. Ferguson, O. Urso, T. Bodrug, B. M. Gassaway, E. R. Watson, J. R. Prabu, P. Lara-Gonzalez, R. C. Martinez-Chacin, D. Y. Wu, K. W. Brigatti, E. G. Puffenberger, C. M. Taylor, B. Haas-Givler, R. N. Jinks, K. A. Strauss, A. Desai, H. W. Gabel, S. P. Gygi, B. A. Schulman, N. G. Brown, A. Bonni, APC7 mediates ubiquitin signaling in constitutive heterochromatin in the developing mammalian brain. *Mol. Cell.* **82**, 90–105.e13 (2022).
55. L. Ledvin, B. M. Gassaway, J. Tawil, O. Urso, D. Pizzo, K. A. Welsh, D. L. Bolhuis, D. Fisher, A. Bonni, S. P. Gygi, N. G. Brown, C. J. Ferguson, The anaphase-promoting complex controls a ubiquitination-phosphoprotein axis in chromatin during neurodevelopment. *Dev. Cell* **58**, 2666–2683.e9 (2023).
56. X. Gong, S. Wang, Q. Yu, M. Wang, F. Ge, S. Li, X. Yu, Cla4 phosphorylates histone methyltransferase Set1 to prevent its degradation by the APC/C^{Cdh1} complex. *Sci. Adv.* **9**, eadi7238 (2023).
57. M. Mazzetto, L. E. Gonzalez, N. Sanchez, V. Reinke, Characterization of the distribution and dynamics of chromatin states in the *C. elegans* germline reveals substantial H3K4me3 remodeling during oogenesis. *Genome Res.* **34**, 57–69 (2024).
58. J. M. Peters, The anaphase promoting complex/cyclosome: A machine designed to destroy. *Nat. Rev. Mol. Cell Biol.* **7**, 644–656 (2006).
59. M. Schwab, A. S. Lutum, W. Seufert, Yeast Hct1 is a regulator of Clb2 cyclin proteolysis. *Cell* **90**, 683–693 (1997).
60. M. Rape, M. W. Kirschner, Autonomous regulation of the anaphase-promoting complex couples mitosis to S-phase entry. *Nature* **432**, 588–595 (2004).
61. J. Hasty, D. McMillen, J. J. Collins, Engineered gene circuits. *Nature* **420**, 224–230 (2002).
62. J. Jeong, J. M. Verheyden, J. Kimble, Cyclin E and Cdk2 control GLD-1, the mitosis/meiosis decision, and germline stem cells in *Caenorhabditis elegans*. *PLOS Genet.* **7**, e1001348 (2011).
63. N. G. Starostina, J. M. Simpliciano, M. A. McGuirk, E. T. Kipreos, CRL2(LRR-1) targets a CDK inhibitor for cell cycle control in *C. elegans* and actin-based motility regulation in human cells. *Dev. Cell* **19**, 753–764 (2010).
64. A. Baudrimont, D. Paouneskou, A. Mohammad, R. Lichtenberger, J. Blundon, Y. Kim, M. Hartl, S. Falk, T. Schedl, V. Jantsch, Release of CHK-2 from PPM-1. D anchorage schedules meiotic entry. *Sci. Adv.* **8**, eabl8861 (2022).
65. D. Hansen, T. Schedl, The regulatory network controlling the proliferation-meiotic entry decision in the *Caenorhabditis elegans* germ line. *Curr. Top. Dev. Biol.* **76**, 185–215 (2006).
66. W. Li, G. Wu, Y. Wan, The dual effects of Cdh1/APC in myogenesis. *FASEB J.* **21**, 3606–3617 (2007).
67. A. Lasorella, J. Stegmüller, D. Guardavaccaro, G. Liu, M. S. Carro, G. Rothschild, L. de la Torre-Ubieta, M. Pagano, A. Bonni, A. Iavarone, Degradation of Id2 by the anaphase-promoting complex couples cell cycle exit and axonal growth. *Nature* **442**, 471–474 (2006).
68. G. Wu, S. Glickstein, W. Liu, T. Fujita, W. Li, Q. Yang, R. Duvoisin, Y. Wan, The anaphase-promoting complex coordinates initiation of lens differentiation. *Mol. Biol. Cell* **18**, 1018–1029 (2007).
69. R. Wäsch, J. A. Robbins, F. R. Cross, The emerging role of APC/CCdh1 in controlling differentiation, genomic stability and tumor suppression. *Oncogene* **29**, 1–10 (2010).
70. S. Dalton, Linking the cell cycle to cell fate decisions. *Trends Cell Biol.* **25**, 592–600 (2015).
71. A. DasGupta, T. L. Lee, C. Li, A. L. Saltzman, Emerging roles for chromo domain proteins in genome organization and cell fate in *C. elegans*. *Front. Cell Dev. Biol.* **8**, 590195 (2020).
72. X. Hou, M. Xu, C. Zhu, J. Gao, M. Li, X. Chen, C. Sun, B. Nashan, J. Zang, Y. Zhou, S. Guang, X. Feng, Systematic characterization of chromodomain proteins reveals an H3K9me1/2 reader regulating aging in *C. elegans*. *Nat. Commun.* **14**, 1254 (2023).
73. S. Brenner, The genetics of *Caenorhabditis elegans*. *Genetics* **77**, 71–94 (1974).
74. C. Frøkjaer-Jensen, M. W. Davis, C. E. Hopkins, B. J. Newman, J. M. Thummel, S. P. Olesen, M. Grunnet, E. M. Jorgensen, Single-copy insertion of transgenes in *Caenorhabditis elegans*. *Nat. Genet.* **40**, 1375–1383 (2008).
75. A. Paix, A. Folkmann, D. Rasoloson, G. Seydoux, High efficiency, homology-directed genome editing in *Caenorhabditis elegans* using CRISPR-Cas9 ribonucleoprotein complexes. *Genetics* **201**, 47–54 (2015).
76. D. Puerta, "Characterization of the regulation of APC/C^{FZR-1} activity in the germline of *Caenorhabditis elegans*," thesis, University of Salamanca, Salamanca, Spain (2023).
77. S. Strome, W. B. Wood, Generation of asymmetry and segregation of germ-line granules in early *C. elegans* embryos. *Cell* **35**, 15–25 (1983).
78. Z. Liu, F. Yuan, J. Ren, J. Cao, Y. Zhou, Q. Yang, Y. Xue, GPS-ARM: Computational analysis of the APC/C recognition motif by predicting D-boxes and KEN-boxes. *PLOS ONE* **7**, e34370 (2012).
79. D. J. Dickinson, A. M. Pani, J. K. Heppert, C. D. Higgins, B. Goldstein, Streamlined genome engineering with a self-excising drug selection cassette. *Genetics* **200**, 1035–1049 (2015).
80. D. T. Byrd, K. Knobel, K. Affeldt, S. L. Crittenden, J. Kimble, A DTC niche plexus surrounds the germline stem cell pool in *Caenorhabditis elegans*. *PLOS ONE* **9**, e88372 (2014).

Acknowledgments: We thank N. Flames (IBV, Valencia) for comments on the manuscript. Also, the contribution of D. Borrego, providing the image of fig. S14A, is acknowledged. Some strains were provided by the CGC, which is funded by the NIH Office of Research Infrastructure Programs (P40 OD010440). **Funding:** This work was supported by the Agencia Estatal de

Investigación of the Spanish Ministry of Science and innovation with grant PID2020-120242GB-I00 (MCIN/AEI /10.13039/501100011033) to J.P.-M., grant PRE2018-083258 to D.P., grant BES-2012-052163 to S.R.-M.; and grant BES-2015-074479 to A.F.-L. S.S.'s laboratory was supported by NIH R01 GM34059. J.K.'s laboratory was supported by NIH R01 GM134119.
Author contributions: Conceptualization: S.S., S.L.C., J.K., and J.P.-M. Methodology: D.P., S.R.-M., A.F.-L., J.K., and J.P.-M. Validation: D.P., S.R.-M., A.F.-L., and J.P.-M. Formal analysis: D.P., S.R.-M., A.F.-L., and J.P.-M. Investigation: D.P., S.R.-M., A.F.-L., and J.P.-M. Resources: S.S., S.L.C., J.K., and J.P.-M. Writing—original draft: J.K. and J.P.-M. Writing—review and editing: D.P., S.R.-M., A.F.-L., S.S., S.L.C., J.K., and J.P.-M. Visualization: J.K. and J.P.-M. Supervision: J.K. and J.P.-M. Project administration: J.K. and J.P.-M. Funding acquisition: J.K. and J.P.-M. **Competing interests:** The authors declare that they have no competing interests. **Data and materials availability:** All data needed to evaluate the conclusions in the paper are present in the paper and/or the Supplementary Materials.

Submitted 24 November 2024
Accepted 25 April 2025
Published 30 May 2025
10.1126/sciadv.adu8572